Dalton Transactions

Cite this: *Dalton Trans.*, 2011, **40**, 8444

www.rsc.org/dalton

PAPER

Biomimetic iron(III) complexes of N_3O and N_3O_2 donor ligands: protonation of coordinated ethanolate donor enhances dioxygenase activity†‡

Karuppasamy Sundaravel,[a] Muniyandi Sankaralingam,[a] Eringathodi Suresh[b] and Mallayan Palaniandavar*[a]

Received 23rd March 2011, Accepted 13th June 2011
DOI: 10.1039/c1dt10495k

A series of iron(III) complexes **1–4** of the tripodal tetradentate ligands *N*,*N*-bis(pyrid-2-ylmethyl)-*N*-(2-hydroxyethyl)amine H(L1), *N*,*N*-bis(pyrid-2-ylmethyl)-*N*-(2-hydroxy- propyl)amine H(L2), *N*,*N*-bis(pyrid-2-ylmethyl)-*N*-ethoxyethanolamine H(L3), and *N*-((pyrid-2-ylmethyl)(1-methylimidazol-2-ylmethyl))-*N*-(2-hydroxyethyl)amine H(L4), have been isolated, characterized and studied as functional models for intradiol-cleaving catechol dioxygenases. In the X-ray crystal structure of [Fe(L1)Cl_2] **1**, the tertiary amine nitrogen and two pyridine nitrogen atoms of H(L1) are coordinated meridionally to iron(III) and the deprotonated ethanolate oxygen is coordinated axially. In contrast, [Fe(HL3)Cl_3] **3** contains the tertiary amine nitrogen and two pyridine nitrogen atoms coordinated facially to iron(III) with the ligand ethoxyethanol moiety remaining uncoordinated. The X-ray structure of the bis(μ-alkoxo) dimer [{Fe(L5)Cl}$_2$](ClO_4)$_2$ **5**, where HL is the tetradentate N_3O donor ligand *N*,*N*-bis(1-methylimidazol-2-ylmethyl)-*N*-(2-hydroxyethyl)amine H(L5), contains the ethanolate oxygen donors coordinated to iron(III). Interestingly, the [Fe(HL)(DBC)]$^+$ and [Fe(HL3)(HDBC)X] adducts, generated by adding ~1 equivalent of piperidine to solutions containing equimolar quantities of iron(III) complexes **1–5** and H_2DBC (3,5-di-*tert*-butylcatechol), display two $DBC^{2-} \rightarrow$ iron(III) LMCT bands (λ_{max}: **1**, 577, 905; **2**, 575,915; **3**, 586, 920; **4**, 563, 870; **5**, 557, 856 nm; $\Delta\lambda_{max}$, 299–340 nm); however, the bands are blue-shifted (λ_{max}: **1**, 443, 700; **2**, 425, 702; **3**, 424, 684; **4**, 431, 687; **5**, 434, 685 nm; $\Delta\lambda_{max}$, 251–277 nm) on adding 1 more equivalent of piperidine to form the adducts [Fe(L)(DBC)] and [Fe(HL3)(HDBC)X]. Electronic spectral and pH-metric titration studies in methanol disclose that the ligand in [Fe(HL)(DBC)]$^+$ is protonated. The [Fe(L)(DBC)] adducts of iron(III) complexes of bis(pyridyl)-based ligands (**1,2**) afford higher amounts of intradiol-cleavage products, whereas those of mono/bis(imidazole)-based ligands (**4,5**) yield mainly the auto-oxidation product benzoquinone. It is remarkable that the adducts [Fe(HL)(DBC)]$^+$/[Fe(HL3)(DBC)X] exhibit higher rates of oxygenation affording larger amounts of intradiol-cleavage products and lower amounts of benzoquinone.

Introduction

Nature typically employs metal centers within enzymes to activate dioxygen and carry out crucial transformations involved in metabolism, mammalian physiology and biodegradation processes.[1–5] The oxidative ring cleavage of catechol and other dihydroxy aromatics is a key step in the biodegradation of naturally occurring aromatic pollutants[1–3] by soil bacteria, which is essential for the global carbon cycle, and have potential utilities in bioremediation efforts. It is catalyzed by the catechol dioxygenase enzymes which can be split into two families: intradiol dioxygenases and extradiol dioxygenases. While the former cleave carbon–carbon bonds between the two catechol oxygens to give muconic anhydride,[6–10] the latter cleave the carbon–carbon bond adjacent to the catechol oxygens to yield 2-hydroxymuconic semialdehyde as the product[11–15] (Scheme 1). The isolated state of the extradiol-cleaving enzymes is characterized by a non-heme iron(II) active site coordinated by the so-called 2-His-1-carboxylate facial triad, consisting of two histidines and one glutamate–aspartate protein residue. The X-ray crystal structure of the isolated intradiol-cleaving protocatechuate 3,4-dioxygenase (3,4-PCD) from *Pseudomonas putida* reveals a trigonal-bipyramidal iron(III) center coordinated to four endogenous protein ligands, namely, H460, H462, Tyr408 and Tyr447.[3,7–9] The fifth coordination position is occupied by a solvent-derived hydroxide ligand. In the substrate activation mechanism[16] proposed already, the hydroxide and the

[a]*Centre for Bioinorganic Chemistry, School of Chemistry, Bharathidasan University, Tiruchirappalli, 620 024, India. E-mail: palanim51@yahoo.com, palaniandavarm@gmail.com; Tel: +91-431-2407053, 2407125*
[b]*Analytical Science Discipline, Central Salt and Marine Chemicals Research Institute, Bhavnagar, 364 002, India*

† Dedicated to Professor C. Natarajan on the occasion of his 80th birthday.

‡ Electronic supplementary information (ESI) available. The results of spectrophotometric titration using triethylamine as a base and pH-metric titration graphs. CCDC reference numbers 819033–819035. For ESI and crystallographic data in CIF or other electronic format see DOI: 10.1039/c1dt10495k

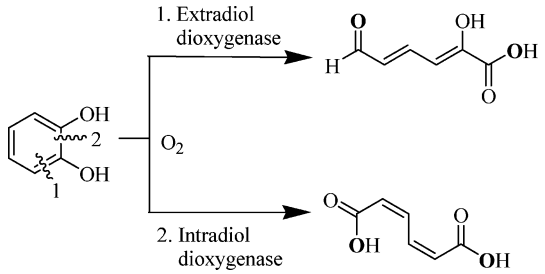

Scheme 1 Mode of cleavage of extradiol and intradiol dioxygenases.

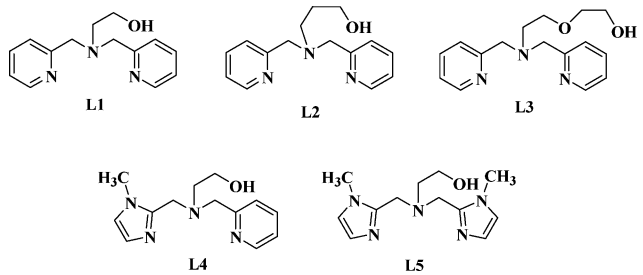

Scheme 3 Ligands employed in this study.

axial Tyr447 unit act as Lewis bases to accept two protons of the catechol substrate and detach from the iron(III) center to form an enzyme–substrate adduct (Scheme 2).[4] Consequently, the coordinated substrate with semiquinone radical character is attacked by dioxygen to form an alkylperoxo intermediate, which is converted into muconic anhydride.[6–10]

Enormous efforts[17–38] have been directed towards the synthesis and characterization of iron(III) complexes of tetradentate linear and tripodal and tetraaza macrocyclic ligands as structural and functional models for the catecholate-iron(III) form of catechol dioxygenases and all these complexes yield mainly intradiol-cleavage products. In our laboratory we have previously investigated many series of iron(III) complexes of tri- and tetradentate ligands with pyridine, (benz)imidazole, phenolate and carboxylate donors, N_2O,[17,27] N_3,[21,28] N_3O,[18,20,29,30] N_2O_2[19,31] and N_4,[32] to closely mimic the structure and function of intra- and extradiol-cleaving catechol dioxygenase enzymes and correlated their reaction rate as well as cleavage yields with the ligand environment. Very recently, we have reported[30] iron(III) complexes of tripodal tetradentate monophenolate and nitrogen donor ligands as models for extradiol-cleaving enzymes and showed that the extradiol cleavage products are obtained in good yields upon adding an equivalent amount of base to the iron(III)-catecholate adduct. Also, the highest extradiol-to-intradiol product selectivity is achieved[32] by using iron(III) complexes of linear tetradentate N_4 ligands in the presence of triethylamine (1.0 equivalent). In our continuous search for more relevant and efficient biomimetic models we have now isolated and characterized a series of iron(III) complexes of systematically varied tripodal tetradentate N_3O (**H(L1)**, **H(L2)**, **H(L4)** and **H(L5)**) and pentadentate N_3O_2 (**H(L3)**) donor ligands (Scheme 3). We wish to understand the role of ligand steric and electronic factors on iron(III) coordination geometry by replacing one or two pyridylmethyl arms in bis(pyrid-2-ylmethyl)-*N*-(hydroxyethyl)amine[38] (**H(L1)**) by 1-methylimidazolylmethyl arms (**H(L4)**, **H(L5)**), and by replacing the ethanol moiety in **H(L1)** by a propanol (**H(L2)**) or ethoxyethanol (**H(L3)**) moiety. The imidazolyl and pyridyl donor atoms mimic the histidine imidazole nitrogen donor function of Tyr447 in the 3,4-PCD enzyme. The ability of the coordinated ethanolate moiety to act as an internal base by abstracting a proton from the catechol substrate makes the iron(III) complexes excellent functional models for the function of axially coordinated Tyr447 in the enzyme. Thus, interestingly, upon protonation of the ethanolate moiety in the catecholate adducts, both the rate of dioxygenation and the yield of intradiol cleavage product increase.

Experimental section

Materials

Pyridine-2-carboxaldehyde, 1-methylimidazole-2-carboxaldehyde, iron(III) perchlorate hydrate, sodium borohydride, sodium triacetoxyborohydride, 3,5-di-*tert*-butylcatechol (H_2DBC), 3-methylcatechol (3-MeH_2CAT), 3-amino-1-propanol, 2(2-aminoethoxy)ethanol (Aldrich), 3,4,5,6-tetrachlorocatechol (H_2TCC) (Lancaster), 2-amino-1-ethanol (Merck, India), catechol (H_2CAT) (Loba, India), iron(III) chloride (anhydrous) (Merck, India) were used as received. The supporting electrolyte *tetra*-*N*-butylammonium perchlorate (Aldrich) was prepared by the procedure reported previously.[39]

Synthesis of ligands

The following general procedure[40] was followed to prepare the ligands **H(L1)**, **H(L2)**, **H(L3)** and **H(L5)**, whereas the ligand **H(L4)** was prepared in two steps.[41]

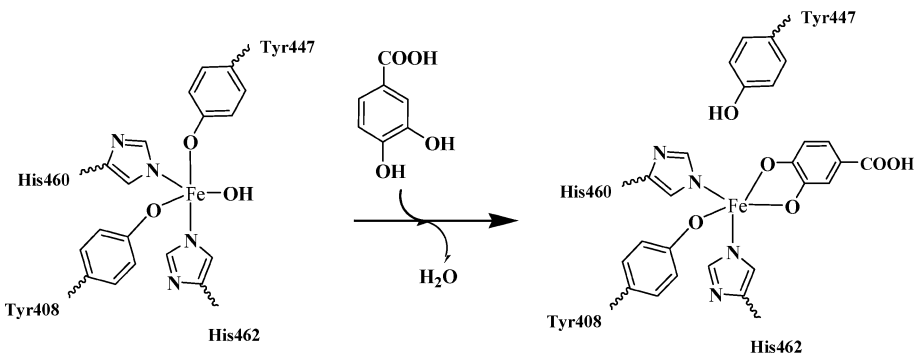

Scheme 2 The proposed substrate-binding process in protocatechuate 3,4-dioxygenase.

***N*,*N*-Bis(pyrid-2-ylmethyl)-*N*-(2-hydroxyethyl)amine H(L1).** To a mixture of 2-amino-1-ethanol (0.12 g, 2 mmol) and pyridine-2-carboxaldehyde (0.43 g, 4 mmol) in dry tetrahydrofuran (30 mL), sodium triacetoxyborohydride (1.69 g, 8 mmol) followed by glacial acetic acid (0.34 mL, 6 mmol) was added under a N_2 atmosphere. The reaction mixture was stirred for 72 h under a N_2 atmosphere. The solvent was removed by rotary evaporation and the residue was dissolved in dichloromethane and then neutralized by the addition of saturated sodium bicarbonate solution (2 × 30 mL). The organic fractions were combined, dried with Na_2SO_4, and the solvent was removed under reduced pressure to obtain the product as a yellow oil (0.41 g, 85%) which was used without further purification for isolation of the complex. ^{1}H NMR (400 MHz, $CDCl_3$): δ = 8.54–8.53 (m, J = 2.8 Hz, 2H), 7.62–7.58 (m, J = 8.6 Hz, 2H), 7.32–7.31 (d, J = 3.8 Hz, 2H), 7.16–7.13 (m, J = 6.2 Hz, 2H), 4.10 (s, 4H), 2.58 (t, J = 5.0 Hz, 2H), 3.65 (t, J = 5.0 Hz, 2H), 2.10 (br s, 1H), ppm. EI-MS m/z = 243 ($C_{14}H_{17}N_3O^+$).

***N*,*N*-Bis(pyrid-2-ylmethyl)-*N*-(2-hydroxypropyl)amine H(L2).** The ligand **H(L2)** (0.42 g, 82%) was synthesized by the procedure described above for the preparation of **H(L1)** except that 3-amino-1-propanol (0.15 g, 2 mmol) was used instead of 2-amino-1-ethanol. ^{1}H NMR (400 MHz, $CDCl_3$): δ = 8.54–8.53 (m, J = 2.0 Hz, 2H), 7.70–7.61 (m, J = 17.4 Hz, 2H), 7.41–7.39 (d, J = 4.0 Hz, 1H), 7.29–7.27 (d, J = 3.6 Hz, 1H), 7.21–7.14 (m, J = 14.6 Hz, 2H), 3.97 (s, 4H), 2.41 (t, J = 6.0 Hz, 2H), 3.58 (t, J = 5.2 Hz, 2H), 1.60 (m, J = 20.2 Hz, 2H), 2.12 (br s, 1H) ppm. EI-MS m/z = 257 ($C_{15}H_{19}N_3O^+$).

***N*,*N*-Bis(pyrid-2-ylmethyl)-*N*-ethoxyethanolamine H(L3).** The ligand **H(L3)** (0.44 g, 77%) was prepared by the same method as that used for **H(L1)** except that 2(2-aminoethoxy)ethanol (0.21 g, 2 mmol) was used instead of 2-amino-1-ethanol. ^{1}H NMR (400 MHz, $CDCl_3$): δ = 8.54–8.50 (dd, J = 2.4, 2.4 Hz, 2H), 7.70–7.63 (m, J = 12.6 Hz, 2H), 7.54–7.52 (d, J = 4.0 Hz, 2H), 7.21–7.14 (m, J = 14.4 Hz, 2H), 3.94 (s, 4H), 3.73 (t, J = 4.4 Hz, 2H), 3.52 (t, J = 5.0 Hz, 2H), 3.49 (t, J = 4.4 Hz, 2H), 2.59 (t, J = 5.0 Hz, 2H), 2.25 (br s, 1H) ppm. EI-MS m/z = 287 ($C_{16}H_{21}N_3O_2^+$).

***N*-((Pyrid-2-ylmethyl)(1-methylimidazol-2-ylmethyl)-*N*-(2-hydroxyethyl)amine H(L4).** The ligand **H(L4)** was prepared in two steps.

Step 1: Synthesis of *N*-pyrid-2-ylmethyl-*N*-(2-hydroxyethyl)-amine[42]. Pyridine-2-carboxaldehyde (0.54 g, 5 mmol) in methanol was added dropwise to 2-amino-1-ethanol (0.31 g, 5 mmol) in methanol (20 mL). The reaction mixture was stirred overnight to get a bright yellow oil. $NaBH_4$ (0.29 g, 7.5 mmol) was then added at 0 °C, the solution was stirred overnight and then rotary evaporated to dryness. The residue was dissolved in water and extracted with dichloromethane and dried with Na_2SO_4. The combined organic layer was rotary evaporated to get *N*-pryidy-2-ylmethyl-*N*-(2-hydroxyethyl)amine as a yellow oil (0.30 g, 40%). ^{1}H NMR (400 MHz, $CDCl_3$): δ = 8.60–7.40 (m, 4H), 4.15 (s, 2H), 2.77 (t, J = 4.2 Hz, 2H), 3.65 (t, J = 5.0 Hz, 2H), 2.20 (br s, 1H), 2.50 (br s, 1H) ppm. EI-MS m/z = 152 ($C_8H_{12}N_2O^+$).

Step 2: Synthesis of *N*-pyrid-2-ylmethyl-*N*-(1-methylimidazol-2-ylmethyl)-*N*-(2-hydroxyethyl)amine. *N*-Pyrid-2-ylmethyl-*N*-(2-hydroxyethyl)amine (0.30 g, 2 mmol) and 1-methylimidazole-2-carboxaldehyde (0.22 g, 2 mmol) were mixed in dry THF (20 mL). Sodium triacetoxyborohydride (1.27 g, 6 mmol) was added to the reaction mixture, followed by glacial acetic acid (0.25 g, 4 mmol). The mixture was then stirred at room temperature for 48 h under nitrogen atmosphere. The solvent was removed and the residue was dissolved in dichloromethane and neutralized with saturated sodium bicarbonate solution. The dichloromethane extract was dried (anhydrous Na_2SO_4) and the solvent was evaporated to give a yellow oil (0.33 g, 67%). The product obtained was used without further purification for the complex preparation. ^{1}H NMR (400 MHz, $CDCl_3$): δ = 8.65–7.40 (m, 4H), 6.75 (d, J = 2.2 Hz, 1H), 6.70 (d, J = 2.2 Hz, 1H), 3.67 (s, 3H), 4.20 (s, 2H), 3.60 (s, 2H) 2.58 (t, J = 4.4 Hz, 2H), 3.63 (t, J = 5.0 Hz, 2H), 2.25 (br s, 1H) ppm. EI-MS m/z = 246 ($C_{13}H_{18}N_4O^+$).

***N*,*N*-Bis(1-methylimidazol-2-ylmethyl)-*N*-(2-hydroxyethyl)-amine H(L5).** The ligand **H(L5)** was prepared by the procedure adopted for the preparation of **H(L1)** except that 1-methylimidazole-2-carboxaldehyde was (0.44 g, 4 mmol) was used instead of pyridine-2-carboxaldehyde to obtain **H(L5)** as a creamy yellow solid (0.36 g, 72%), which is pure enough for the preparation of the iron(III) complex. ^{1}H NMR (400 MHz, $CDCl_3$): δ = 6.80 (d, J = 2.6 Hz, 2H), 6.68 (d, J = 2.2 Hz, 2H), 3.64 (s, 6H), 3.60 (s, 4H), 2.55 (t, J = 3.8 Hz, 2H), 3.67 (t, J = 4.4 Hz, 2H), 2.0 (b s, 1H) ppm. EI-MS m/z = 249 ($C_{12}H_{19}N_5O^+$).

Synthesis of iron(III) complexes

Caution: Perchlorate salts of metal complexes with organic ligands are potentially explosive and should be handled with great care.

[Fe(L1)Cl$_2$] 1. $FeCl_3$ (0.16 g, 1 mmol) in methanol (10 mL) was added to a solution of **H(L1)** (0.24 g, 1 mmol) in methanol (10 mL), stirred well and then cooled. The yellow complex (0.30 g, 82%) was filtered off, washed with small amounts of cold methanol and dried under vacuum. Yellow crystals of [Fe(L1)Cl_2] **1** suitable for X-ray diffraction was obtained by slow evaporation of acetonitrile : methanol (1 : 1, v/v) solution. Anal. Calcd for $C_{14}H_{16}N_3FeCl_2O$ (369): C, 45.56; H, 4.37; N, 11.39. Found: C, 45.58; H, 4.41; N, 11.42. ESI-MS m/z = 333 ($C_{14}H_{16}N_3OFeCl^+$).

[Fe(L2)Cl$_2$] 2. The complex **2** (0.31 g, 79%) was prepared by using the procedure employed for isolating **1**. Anal. Calcd for $C_{15}H_{18}N_3FeCl_2O$ (383): C, 47.03; H, 4.74; N, 10.97. Found: C, 47.05; H, 4.79; N, 11.01. ESI-MS m/z = 347 ($C_{15}H_{18}N_3OFeCl^+$).

[Fe(HL3)Cl$_3$] 3. A procedure analogous to that used to prepare **1** was adopted, using anhydrous $FeCl_3$ (0.16 g, 1 mmol) and H(L3) (0.28 g, 1 mmol) instead of H(L1). The solution was stirred which resulted in the formation of yellow colored precipitate (0. 31 g 70%) after one hour and it was filtered off. Anal. Calcd. for $C_{16}H_{21}N_3O_2FeCl_3$ (449.56): C, 42.75; H, 4.71; N, 9.35. Found: C, 42.77; H, 4.72; N, 9.39. X-Ray diffraction quality crystals of **3** were obtained by the vapour diffusion of diethylether into the complex dissolved in methanol : acetonitrile (2 : 1, v/v) solvent mixture. ESI-MS m/z = 414 ($C_{16}H_{21}N_3O_2FeCl_2^+$).

[Fe(L4)Cl$_2$] 4. The complex **4** (0.23 g, 63%) was also prepared by using the procedure employed for isolating [Fe(L1)Cl_2]. Anal. Calcd for $C_{13}H_{17}N_4FeCl_2O$ (372): C, 41.97; H, 4.61; N,

15.06. Found: C, 41.99; H, 4.64; N, 15.08. ESI-MS m/z = 337 ($C_{13}H_{17}N_4OFeCl^+$).

[{Fe(L5)Cl}$_2$](ClO$_4$)$_2$ 5. **H(L5)** (0.25 g, 1 mmol) in ethanol (5 mL) was added to a solution of $FeCl_3$ (0.11 g, 0.66 mmol) and $Fe(ClO_4)_3$ (0.12 g, 0.33 mmol) in ethanol/methanol (5 + 5 mL), stirred well and then cooled. The yellow complex (0.33 g, 75%) was filtered off, washed with small amounts of cold methanol and dried under vacuum. Anal. Calcd for $C_{24}H_{36}Cl_4Fe_2N_{10}O_{10}$ (878.11): C, 32.83; H, 4.13; N, 15.95. Found: C, 32.85; H, 4.17; N, 15.99. Red-orange crystal of [{Fe(L5)Cl}$_2$](ClO4)$_2$ **5** suitable for X-ray diffraction was obtained by slow evaporation of acetonitrile : methanol (2 : 1, v/v) solution layered with diethylether.

Physical measurements

Elemental analyses were performed on a Perkin Elmer Series II CHNS/O analyzer 2400. The electronic spectra were recorded on a Agilent 8453 diode array spectrophotometer (wavelength range 1100–190 nm). The pH titration was monitored using a Toshniwal (CL 54) pH meter equipped with a combination pH electrode. Cyclic voltammetry (CV) and differential pulse voltammetry (DPV) were performed using a three-electrode cell configuration. A platinum sphere, platinum plate and Ag(s)/$AgNO_3$ were used as working, auxiliary and reference electrodes respectively. The supporting electrolyte used was NBu_4ClO_4. The platinum sphere electrode was sonicated for two minutes in dilute nitric acid, dilute hydrazine hydrate and then in double distilled water to remove the impurities. The temperature of the electrochemical cell was maintained at 25.0 ± 0.2 °C by a cryocirculator (HAAKE D8 G). The solutions were deoxygenated by bubbling research grade nitrogen and an atmosphere of nitrogen was maintained over the solution during measurements. The $E_{1/2}$ values were observed under identical conditions for various scan rates. The instruments utilized included an EG & G PAR 273 Potentiostat/Galvanostat and Pentium IV computer along with EG & G M270 software to carry out the experiments and to acquire the data. ^{1}H NMR spectra were recorded on a Bruker 400 MHz spectrometer. The cleavage products were analyzed using Hewlett Packard (HP) 6890 Gas Chromatograph (GC) series equipped with a Flame Ionization Detector (FID) and a HP-5 capillary column (30 m × 0.32 mm × 2.5 μm). GC-MS analysis was performed on a Agilent 7890A GC System and 5975C inert MSD with Triple-Axis Detector GC-MS (Electron Ionization) instrument using a HP-5 capillary column.

Data collection and structure refinement

Suitable single crystals were grown by slow evaporation of the acetonitrile/methanol solution of complexes at 4 °C. A crystal of suitable size selected from the mother liquor was immersed in paraffin oil, then mounted on the tip of a glass fiber and cemented using epoxy resin. Intensity data for the crystal were collected using Mo-Kα (λ = 0.71073 Å) radiation on a Bruker SMART APEX diffractometer equipped with a CCD area detector at 100 K. The crystallographic data are listed in Table 1. The SMART[43] program was used for collecting frames of data, indexing the reflections, and determination of lattice parameters; SAINT[43] program for integration of the intensity of reflections and scaling; SADABS[44] program for absorption correction, and the SHELXTL[45] program for space group and structure determination, and least-squares refinements on F^2. The structure was solved by heavy atom method. Other non-hydrogen atoms were located in successive difference Fourier syntheses. The final refinement was performed by full-matrix least-squares analysis. Hydrogen atoms of the ligand

Table 1 Crystal data and structure refinement details for [Fe(L1)Cl$_2$] **1**, [Fe(H(L3))Cl$_3$] **3** and [{Fe(L5)Cl}$_2$](ClO$_4$)$_2$ **5**

	1	**3**	**5**
Empirical Formula	$C_{28}H_{32}Cl_4Fe_2N_6O_5$	$C_{16}H_{21}Cl_3FeN_3O_2$	$C_{24}H_{36}Cl_4Fe_2N_{10}O_{10}$
Formula Weight	786.10	449.56	878.13
Crystal System	Monoclinic	Monoclinic	Monoclinic
Crystal Size (mm)	0.31 × 0.18 × 0.12	0.34 × 0.18 × 0.08	0.52 × 0.27 × 0.04
Space group	$P2_1$	$P2_1/c$	$P2_1/c$
a, (Å)	7.0402(6)	7.358(8)	8.1513(7)
b, (Å)	15.9083(14)	19.495(19)	12.0527(10)
c, (Å)	17.0698(15)	13.953(15)	17.3786(15)
α, (°)	90	90	90
β, (°)	94.596(2)	103.352(17)	90.6750(10)
γ, (°)	90	90	90
V (Å^3)	1905.6(3)	1947(4)	1707.2(3)
Z	2	4	2
Temperature, (K)	100	100	100
ρ (calc), (g cm^{-3})	1.370	1.533	1.708
Radiation Mo-Kα (λ/Å)	0.71073	0.71073	0.71073
Goodness of fit on F^2	1.117	1.16	1.09
Number of reflections measured	11498	9901	10085
Number of reflections used	7510	3817	3939
Number of refined parameters	406	227	228
R(int)	0.0303	0.0882	0.029
Final R indices [$I > 2\sigma(I)$]	R_1 = 0.0627; wR_2 = 0.1532	R_1 = 0.0813; wR_2 = 0.1674	R_1 = 0.0606; wR_2 = 0.1552
R indices (all data)	R_1 = 0.0665; wR_2 = 0.1558	R_1 = 0.1141; wR_2 = 0.1837	R_1 = 0.0686; wR_2 = 0.1600

[a] $R1 = [\Sigma(||Fo|-|Fc||)/\Sigma|Fo|]$, [b] $wR2 = \{[\Sigma(w(Fo^2-Fc^2)^2)/\Sigma(wFo^4)]^{1/2}\}$

moiety were fixed in calculated positions and then refined using a riding model.

Spectrophotometric titration

Spectrophotometric titration was carried out to gain a knowledge about the influence of added base on the iron(III)–catecholate adduct formation and also, to attain the optimized conditions for catechol cleavage by O_2, it is necessary to provide a high concentration of the mononuclear iron complex with one coordinated catecholate dianion. To determine these ideal conditions for dioxygenase activity, spectrophotometric titrations were performed as described previously.[46–48] A methanol solution of H_2DBC (20 μL, 2×10^{-2} M) was added to a solution of complexes **1–4** (2×10^{-4} M) and complex **5** (1×10^{-4} M) in methanol (2 mL). The resulting solution was titrated with portions of 0.2 equivalents of piperidine (4 μL, 2×10^{-2} M) in methanol, and the electronic absorption spectra were monitored. To avoid the decomposition of the catecholate adduct, the titration was performed under a N_2 atmosphere and repeated three times to obtain a concordant value.

Reactivity studies and determination of cleavage products

The catechol cleavage activity of all the complexes toward H_2DBC was examined in the methanol solution of the iron(III) complexes as described for spectrophotometric titration,[46–48] except that the O_2 saturated methanol[22,49] was used. The iron(III)–DBC^{2-} adduct generated *in situ* upon the addition of 0.8 equivalents of piperidine to the methanol solution of **1** and **2**, 0.7 equivalents of piperidine was used for complexes **4** and **5** and exactly 1.0 equivalent of base is required for **3**, with 2.0 equivalents of piperidine. The reaction of complex–substrate adducts with oxygen was monitored by following the disappearance of the DBC^{2-}–iron(III) ligand-to-metal charge transfer (LMCT) band at 25 °C.

The product analysis was carried out by stirring the methanolic (20 mL) solution of complexes **1–4** (0.05 mmol) and **5** (0.025 mmol), H_2DBC (0.05 mmol) and the appropriate amount of base (piperidine) as determined from spectrophotometric titration was added to the solution under molecular oxygen over 12 h at room temperature. The oxygenation reaction was quenched by the addition of 6 M HCl (5 mL) and the products were extracted from the aqueous solution with diethylether (3 × 20 mL). The clear yellow organic layer was separated and dried over anhydrous sodium sulfate at room temperature. Further purification of the products was accomplished by column chromatography using silica gel and CH_2Cl_2 : CH_3OH (4 : 1, v/v) solvent mixture as the eluent. The major products were separated and analyzed by GC, GC-MS and ^{1}H NMR techniques. The other minor products were analyzed as a mixture, detected by GC-MS (EI) and quantified using GC (FID) with the following temperature program: injector temperature 130 °C; initial temperature 60 °C, heating rate 10 °C min^{-1} to 130 °C, then increasing at a rate 2 °C min^{-1} to 160 °C and then increasing at a rate 5 °C min^{-1} to 260 °C; FID temperature 280 °C. GC-MS analysis was performed under conditions identical to those used for GC analysis and the oxygenation products identified by comparing with the retention times reported previously.[20,22,29,38]

Results and discussion

Syntheses of ligands and iron(III) complexes

All of the ligands **H(L1)–H(L5)** were synthesized by adopting known literature procedures[40–42] which involve the reductive amination of the corresponding aldehyde with amino alcohol in the presence of sodium triacetoxyborohydride and glacial acetic acid. They were reacted with equimolar amounts of iron(III) salt in methanol to obtain complexes **1–5**. On the basis of the results of elemental analysis, the formulae of the iron(III) complexes **1**, **2** and **4** are represented as $[Fe(L)Cl_2]$, **3** as $[Fe(HL)Cl_3]$ and **5** as $[\{Fe(L)Cl\}_2](ClO_4)_2$, which is supported by the X-ray crystal structures of $[Fe(L1)Cl_2]$ **1**, $[Fe(HL3)Cl_3]$ **3** and $[\{Fe(L5)Cl\}_2](ClO_4)_2$ **5**, respectively.

The ESI-MS profile of the dinuclear complex **5** in methanol solution shows a peak only for the mononuclear species $[Fe(L5)Cl]^+$ (ESI-MS: m/z = 339 ($C_{12}H_{18}N_5OFeCl^+$)) (Scheme 4), suggesting dissociation of the dinuclear complex into a mononuclear species in solution.[38] The present iron(III) complexes have magnetic moments in the range 5.45–5.65 BM at room temperature, which is characteristic of a high-spin iron(III) center.[18–20,22]

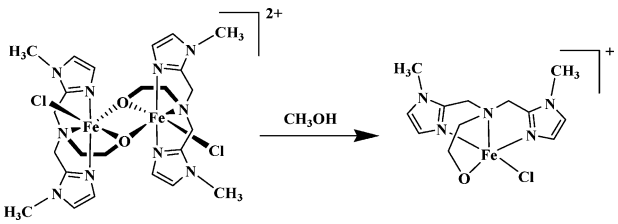

Scheme 4 Formation of mononuclear $[Fe(L5)Cl]^+$ species from the dinuclear complex $[\{Fe(L5)Cl\}_2]^{2+}$.

Description of crystal structures of $[Fe(L1)Cl_2]$ 1, $[Fe(H(L3))Cl_3]$ 3 and $[\{Fe(L5)Cl\}_2](ClO_4)_2$ 5

The thermal ellipsoid plot of complex **1** is depicted in Fig. 1, and the selected bond distances and angles are collected in Table 2. The bond angles Cl1–Fe1–N2 (166.79(15)°),

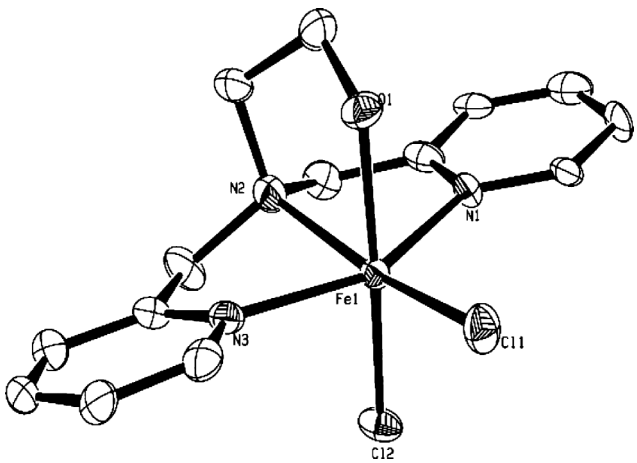

Fig. 1 ORTEP diagram of complex $[Fe(L1)Cl_2]$ **1** showing 50% probability thermal ellipsoids and labeling scheme for selected atoms. All the hydrogen atoms are omitted for clarity. Only one component of the Asymmetric Unit is shown.

Table 2 Selected bond lengths [Å] and bond angles [deg] for [Fe(L1)Cl_2] **1**, [Fe(H(L3))Cl_3] **3** and [(Fe(L5)Cl)$_2$]$(ClO_4)_2$ **5**

1		**3**		**5**	
Fe(1)–Cl(1)	2.2264(17)	Fe(1)–Cl(1)	2.323(3)	Fe(1)–Cl(1)	2.3135(10)
Fe(1)–Cl(2)	2.2712(15)	Fe(1)–Cl(2)	2.348(3)	Fe(1)–O(1)	2.028(3)
Fe(1)–O(1)	2.090(4)	Fe(1)–Cl(3)	2.312(2)	Fe(1)–N(1)	2.067(3)
Fe(1)–N(1)	2.121(5)	Fe(1)–N(1)	2.157(5)	Fe(1)–N(3)	2.360(3)
Fe(1)–N(2)	2.216(5)	Fe(1)–N(2)	2.319(5)	Fe(1)–N(5)	2.053(3)
Fe(1)–N(3)	2.122(5)	Fe(1)–N(3)	2.209(5)	Fe(1)–O(1_a)	1.921(2)
Cl(1)–Fe(1)–Cl(2)	100.70(6)	Cl(1)–Fe(1)–Cl(2)	96.32(7)	Cl(1)–Fe(1)–O(1)	166.80(8)
Cl(1)–Fe(1)–O(1)	88.92(13)	Cl(1)–Fe(1)–Cl(3)	99.28(9)	Cl(1)–Fe(1)–N(1)	90.48(9)
Cl(1)–Fe(1)–N(1)	105.18(15)	Cl(1)–Fe(1)–N(1)	87.56(14)	Cl(1)–Fe(1)–N(3)	114.74(8)
Cl(1)–Fe(1)–N(2)	166.79(15)	Cl(1)–Fe(1)–N(2)	93.94(13)	Cl(1)–Fe(1)–N(5)	90.50(10)
Cl(1)–Fe(1)–N(3)	100.82(15)	Cl(1)–Fe(1)–N(3)	166.39(13)	Cl(1)–Fe(1)–O(1_a)	95.22(8)
Cl(2)–Fe(1)–O(1)	169.75(13)	Cl(2)–Fe(1)–Cl(3)	95.78(7)	O(1)–Fe(1)–N(1)	97.48(12)
Cl(2)–Fe(1)–N(1)	90.93(13)	Cl(2)–Fe(1)–N(1)	168.51(14)	O(1)–Fe(1)–N(3)	77.74(10)
Cl(2)–Fe(1)–N(2)	92.16(15)	Cl(2)–Fe(1)–N(2)	91.04(14)	O(1)–Fe(1)–N(5)	88.73(12)
Cl(2)–Fe(1)–N(3)	92.55(14)	Cl(2)–Fe(1)–N(3)	88.92(14)	O(1)–Fe(1)–O(1_a)	72.41(11)
O(1)–Fe(1)–N(1)	83.08(17)	Cl(3)–Fe(1)–N(1)	94.25(14)	N(1)–Fe(1)–N(3)	73.98(12)
O(1)–Fe(1)–N(2)	78.45(19)	Cl(3)–Fe(1)–N(2)	164.34(13)	N(1)–Fe(1)–N(5)	146.11(13)
O(1)–Fe(1)–N(3)	89.05(17)	Cl(3)–Fe(1)–N(3)	92.64(15)	O(1_a)–Fe(1)–N(1)	107.07(12)
N(1)–Fe(1)–N(2)	77.39(19)	N(1)–Fe(1)–N(2)	77.88(19)	N(3)–Fe(1)–N(5)	74.91(12)
N(1)–Fe(1)–N(3)	152.60(2)	N(1)–Fe(1)–N(3)	85.02(18)	O(1_a)–Fe(1)–N(3)	150.04(11)
N(2)–Fe(1)–N(3)	75.35(19)	N(2)–Fe(1)–N(3)	73.36(18)	O(1_a)–Fe(1)–N(5)	106.57(12)

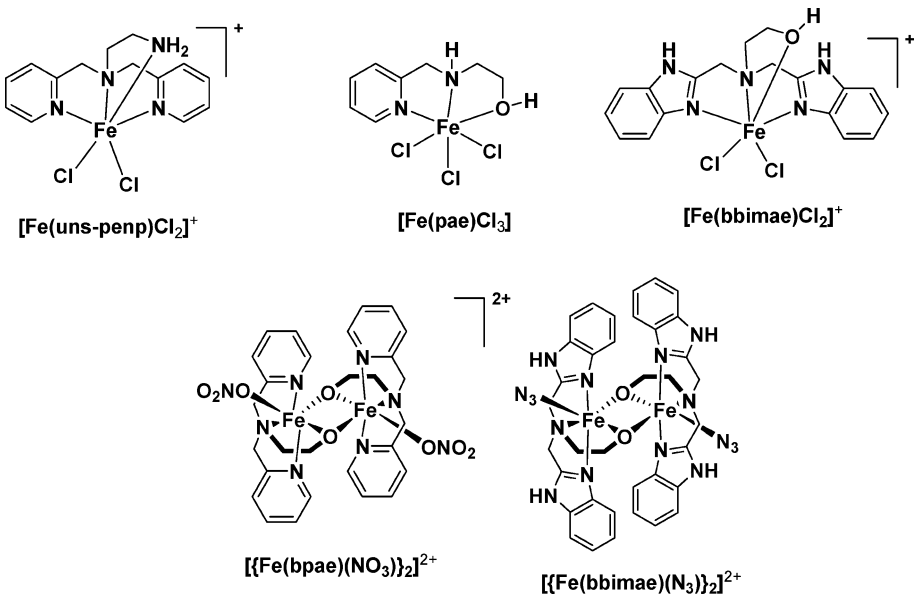

Scheme 5 Iron(III) complexes used for structural comparison.

Cl2–Fe1–O1 (169.75(13)°) and N1–Fe1–N3 (152.60(2)°) deviate markedly from that of the ideal octahedron (180°), suggesting distortion in the octahedral coordination geometry.[18–20,22,29,47] The Fe–N_{py} bond distances (Fe–N1, 2.121(5); Fe–N3, 2.122(5) Å) fall in the range of Fe–N_{py} bond distances reported[18–20,22,29,47] previously, but are significantly shorter than the Fe–N_{py} bond distances (2.127(2), 2.136(2) Å) observed[47] in the analogous complex [Fe(uns-penp)Cl_2]ClO_4, where uns-penp = bis(2-pyridyl)methyl)ethylenediamine (Scheme 5). Also, the Fe–N_{amine} distance is considerably longer than the Fe–N_{py} distance, suggesting a relatively weak iron(III)–tertiary amine nitrogen overlap. The Fe–N_{amine} bond (2.216(5) Å) is longer than the Fe–N_{py} bonds due to sp^3 and sp^2 hybridizations of the amine and pyridine nitrogen atoms, respectively.[18–20,22,47] The Fe–$O_{ethanolate}$ bond distance (2.090(4) Å) is intermediate between those observed for ethoxyl (–$(CH_2)_2$–OH) (2.131(2) Å) and bridged-ethanolate (2.013(2), 2.028(2) Å) oxygen donor atom respectively of the complexes [Fe(pae)Cl_3], where pae = *N*-(pyrid-2-ylmethyl)-2-hydroxyethylamine[42] and [Fe(bbimae)Cl_2]Cl, where bbimae = bis(benzimidazol-2-yl-methyl)(2-hydroxyethyl)amine,[22] and the complex [{Fe(bpae)(NO_3)}$_2$]$(NO_3)_2$, where bpae = *N*,*N*-bis(2-pyridylmethyl)-*N*-(2-hydroxyethyl)amine.[38]

The ORTEP plot of the complex [Fe(H(L3))Cl_3] **3** is shown in Fig. 2 with the atom numbering scheme. The selected bond lengths and angles are listed in Table 2. The iron(III) center in the complex is facially coordinated to two pyridine and one tertiary amine nitrogens of theH(L3) ligand and the three chloride ions occupy the remaining octahedral sites, and the ligand

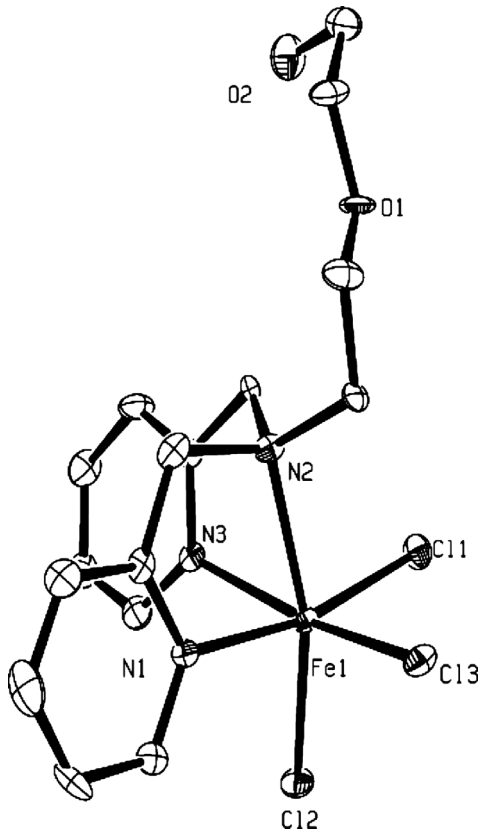

Fig. 2 ORTEP diagram of complex $[Fe(H(L3))Cl_3]$ **3** showing 50% probability thermal ellipsoids and labeling scheme for selected atoms. All the hydrogen atoms are omitted for clarity.

ethoxyethanol moiety is not coordinated. The N–Fe–N bond angles (Table 2) deviate from the ideal value of 90°, revealing that the coordination octahedron is distorted. As discussed above, the Fe–N_{amine} (2.319(5) Å) bond distance is much longer than the Fe–N_{py} bond distances (2.157(5), 2.209(5) Å). It is also longer than those reported (Fe–N_{amine}, 2.211(5) – 2.281(2) Å)[28] previously for the iron(III) complexes of the type $[Fe(L)Cl_3]$. The distance between the pyridine nitrogens and the iron core fall within the range reported[21,22,28,47,50] previously.

The ORTEP representation of the dialkoxo-bridged dinuclear complex cation $[\{Fe(L5)Cl\}_2]^{2+}$ **5** is depicted in Fig. 3, with selected bond distances and angles presented in Table 2. Each iron(III) center in **5** adopts a distorted octahedral coordination geometry defined by the N_3O_2 donor set of the tetradentate ligand **L5** and a Cl^- ion. The amine nitrogen and bridged ethanolate oxygen atoms lie in the plane of the Fe_2O_2 core.[38] The two imidazole nitrogen atoms occupy the two apical positions in the octahedron, the chloride ion is located *trans* to the ethanolate bridge and the sixth coordination position is completed by the ethanolate oxygen atom of the other ligand. The Fe–N_{amine} bond length (2.360(3) Å) is longer than the average bond length of the Fe–N_{im} bond (N1, 2.067(3); N5, 2.053(3) Å) reported for the analogous diiron(III) complexes of the tetradentate ligands containing bis-pyridine[38] and bis-benzimidazole[51,52] donor moieties. The Fe–O_{alkoxo} bonds (O1, 2.028(3); O1_a, 1.921(2) Å)) are uneven, forming the asymmetric Fe_2O_2 core of **5** with different Fe(1)–O(1)–Fe(1_a) (107.59(11)°) and O(1)–Fe(1)–O(1_a) (72.41(11)°) bond angles.[38]

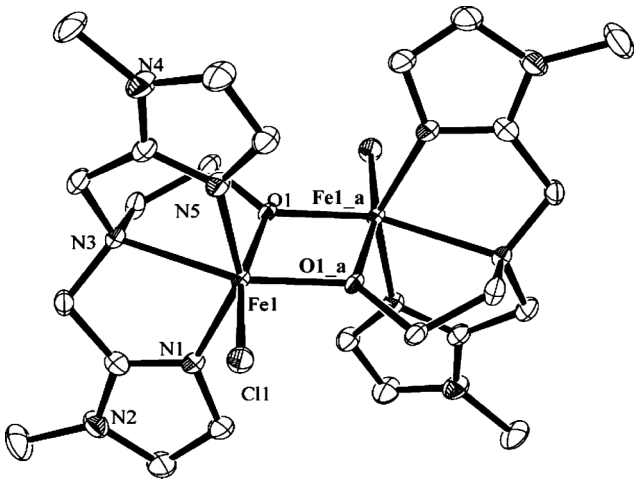

Fig. 3 ORTEP diagram of dinuclear complex cation $[\{Fe(L5)Cl\}_2]^{2+}$ **5** showing 50% probability thermal ellipsoids and labeling scheme for selected atoms. All the hydrogen atoms and perchlorate anions are omitted for clarity.

Electronic absorption spectra

All the complexes show an intense absorption band around 360 nm (Table 3), which can be assigned to the charge-transfer transition from Cl^- to iron(III).[18–20,29] When 3,5-di-*tert*-butylcatechol (H_2DBC), pretreated with two equivalents of piperidine, is added to **1–5** in methanol solution, two new bands appear in the visible region (557–586, 685–702 nm, Table 3), which are assignable to DBC^{2-}-to-iron(III)(dπ*) LMCT transitions[22–31,48,53] involving two different catecholate orbitals on the chelated DBC^{2-}. The energy of the low-energy LMCT band of the adducts show a remarkable dependence on the nature of the primary ligands,[23–26] **1** ~ **2** < **3**; **1** < **4** ~ **5**. On replacing the ethanolate donor in **1** by the propanolate donor arm as in **2**, no appreciable change in the catecholate-to-iron(III) charge-transfer (LMCT) transitions (**1**, 700 nm; **2**, 702 nm) is observed, suggesting that the electronic environment around iron(III) in them is the same (*cf.* below). The replacement of the ethanolate arm in **1** by an ethoxyethanol arm, as in **3**, is expected to increase the Lewis acidity of the metal center and shift the low-energy LMCT transition to lower energy as both the ether and hydroxyl oxygen atoms are not coordinated to the iron(III) center (*cf.* above). A blue-shift is observed indicating that the electrophilicity of the iron(III) center in the adduct of **3** is compensated by a chloride ion. The increase in negative charge on the iron(III) center on replacing one/both of the pyridyl moieties in **1** by the more Lewis basic 1-methylimidazolyl arm(s) [pK_a (BH^+): 1-methylimidazole, 7.2; pyridine, 5.6][54] to obtain **4**/**5** raises the energy of the iron(III) dπ* orbital, leading to higher LMCT band energies. Thus the Lewis acidity of the iron(III) center in the catecholate adduct is modified upon changing the ligand environment.

To gain an insight into the role of ethanolate coordination on catecholate adduct formation, an equimolar mixture of **1–5** and H_2DBC in methanol was titrated with the base piperidine (Scheme 6). Upon addition of 0.2–0.4 equivalents of piperidine (Fig. 4A) or Et_3N (Figure S1, ESI‡), two moderately intense DBC^{2-}-to-iron(III)(dπ*) LMCT bands[17–22,25,46–48,53] appear around

Table 3 Electronic spectral data for iron(III) complexes[a] **1–5** and their 3,5-di-*tert*-butyl-catecholate (DBC^{2-}) adducts[b,c] in methanol solution

λ_{max}, nm (ε, M^{-1} cm^{-1})					
Added ligands	$[Fe(L1)Cl_2]$	$[Fe(L2)Cl_2]$	$[Fe(H(L3))Cl_3]$	$[Fe(L4)Cl_2]$	$[Fe(L5)Cl_2]$
None	357 (2 220)	354 (10 980)	331 (8420)	359 (10 820)	363 (4 220)
	314 (3 290)	317 (14 040)	253 (10 900)	317 (19 610)	293 (6 780)
$HDBC^-$	905 (1315)	915 (2380)	920 (2085)	870 (1455)	856 (1310)
	577 (865)	575 (1469)	586 (1400)	563 (875)	557 (855)
DBC^{2-}	700 (2355)	702 (1860)	684 (1720)	687 (1915)	685 (1665)
	443 (1440)	425 (1330)	424 (1260)	431 (1140)	434 (1100)

[a] Concentration of iron(III) complexes: 2×10^{-4} M. [b] The adducts [Fe(HL)(DBC)] were generated by adding one equivalent of H_2DBC pretreated with 0.7–1.0 equivalent of piperidine (see text). [c] The adducts [Fe(L)(DBC)] were generated by adding one equivalent of H_2DBC pretreated with two equivalents of piperidine.

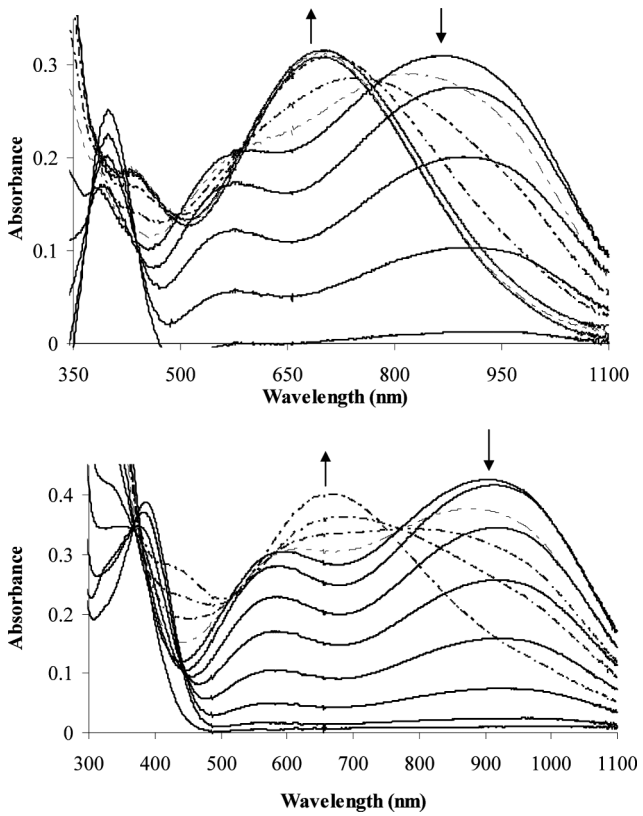

Fig. 4 (A) Spectrophotometric titration of a solution of equimolar amounts of $[Fe(L1)Cl_2]$ **1**(2×10^{-4} M), and 3,5-di-*tert*-butylcatechol (H_2DBC) against piperidine in methanol. Solid line: 0.0–0.8 equiv.; dashed line: 1.0–2.0 equiv. (B) Spectrophotometric titration of a solution of equimolar amounts of $[Fe(HL3)Cl_3]$ **3** (2×10^{-4} M), and (H_2DBC) 3,5-di-*tert*-butylcatechol against piperidine in methanol. Solid line: 0.0–1.2 equiv.; dashed line: 1.4–2.0 equiv.

577 and 905 nm for **1**. When a greater amount of base (0.4–0.8 equivalent) is added, both the bands significantly increase in absorption intensity, suggesting the formation of increasing amounts of the mononuclear adduct $[Fe(\mathbf{HL}1)(DBC)]^+$. On adding a greater amount of base (0.8–2.0 equivalents), the low-energy LMCT band starts shifting to higher energy and finally two new bands (443, 700 nm) appear. When the second equivalent of piperidine is added, the bound ethanol moiety is deprotonated to form the adduct species [Fe(L1)(DBC)] and the coordination of ethanolate to iron(III) builds up a higher electron density on the iron(III) center, causing the LMCT bands to shift to higher energies.[20,24,25,32] The band positions obtained are the same as those observed (Table 3) when DBC^{2-}, generated by adding two equivalents of piperidine or Et_3N, is added to $[Fe(L1)Cl_2]$, confirming the formation of [Fe(L1)(DBC)]. The complex species $[Fe(L1)(MeOH)_2]^{2+}$, generated by treating $[Fe(L1)Cl_2]$ with two equivalents of anhydrous $AgClO_4$, was used for the spectral titration with piperidine or Et_3N and similar results were obtained. Similar results were also obtained for **2**, **4** and **5**; however, different amounts of piperidine (**2**, 0.8; **4** & **5**, 0.7) are required to form the adduct $[Fe(HL)(DBC)]^+$. Also, similar changes in spectral bands are observed when one mole of $HClO_4$ is added prior to the spectral titration, but as expected, higher amounts of base are needed. Interestingly, upon adding one equivalent of H_2DBC to $[Fe(HL3)Cl_3]$ **3** (or $[Fe(HL3)(MeOH)_3]^{3+}$), two LMCT bands appear around 586 and 920 nm (Fig. 4B), even in the absence of added base. Upon addition of 0.2–1.0 equivalents of piperidine or Et_3N, both bands significantly increase in absorption intensity, suggesting the formation of increasing amounts of the adduct $[Fe(HL3)(HDBC)X]^+$ (X = Sol, Cl). Addition of even greater amounts of base (1.2–2.0 equiv.) shifts the LMCT bands to higher energy and finally two new bands (424, 684 nm) appear, suggesting the formation of [Fe(HL3)(DBC)X] species (Scheme 6).[18–25,32]

The energy of the low-energy LMCT bands observed for $[Fe(HL)(DBC)]^+$/[Fe(HL3)(HDBC)X] species, generated upon addition of 0.7–1.0 equivalents of piperidine in methanol solution, varies in the order: **1** > **2** > **3**; **1** < **4** < **5**. The decrease in energy of the band reflects the increase in Lewis acidity of the iron(III) center in this order, as modified by the ligand donor moieties.[17–22,25,53] The position of the high-energy band also depends on the nature of ligand donors. The lone pair orbital on the propanolate oxygen atom in the DBC^{2-} adduct of **2** is expected to be oriented not exactly towards the iron(III) orbital, causing a decrease in negative charge built on iron(III) and stabilizing the $d\pi^*$ orbitals of iron(III) and leading to a decrease in energy gap between the $d\pi^*$ orbital and ligand catecholate orbitals. Hence, the observed LMCT band energy is lower than that for **1**.[17–22,25,37,53] The increase in negative charge on the iron(III) center upon replacing one/two pyridyl donors in the DBC^{2-} adduct of **1** by the more basic 1-methylimidazole moiety, as in the adducts of **4** and **5**, leads to an enhancement of the energy of the LMCT bands, as observed for

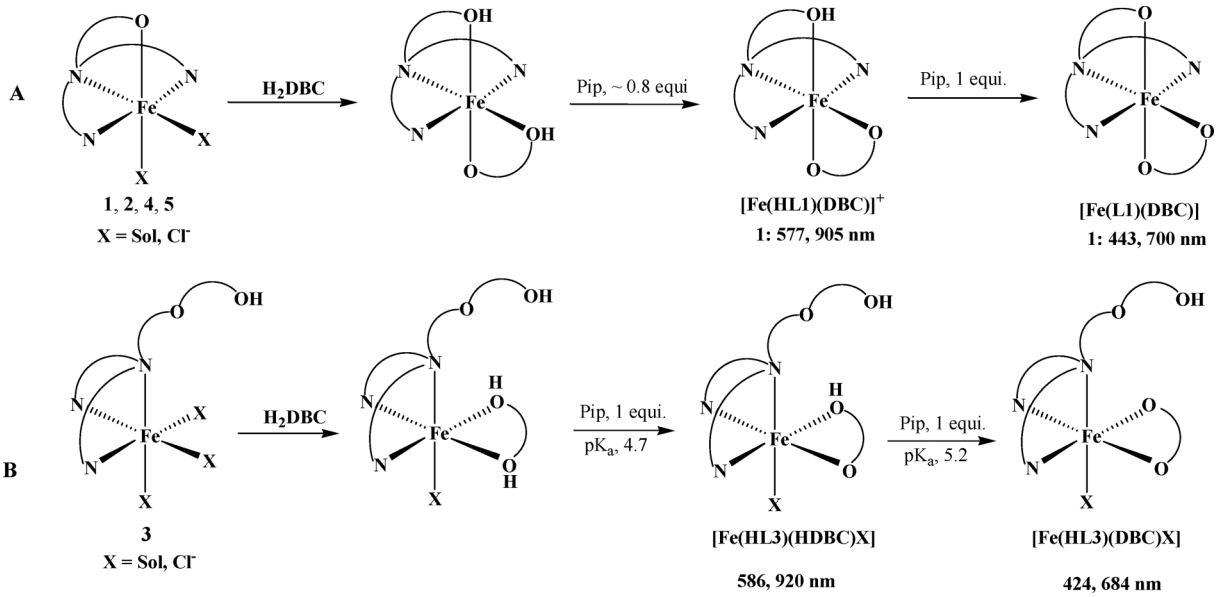

Scheme 6 Effect of piperidine on catecholate adduct formation.

[Fe(L)(DBC)] adducts (*cf.* above). The LMCT bands observed for the catecholate adduct $[Fe(HL3)(HDBC)X]^+$ are lower in energy than those observed for the corresponding adducts of **1** and **2**. This illustrates that the ethoxyethanol moiety is not deprotonated and hence the Lewis acidity of the iron(III) center is higher.

pH-metric titration

When **1** is treated with one equivalent each of $HClO_4$ and H_2DBC in methanol and then titrated with piperidine or Et_3N, interesting results are obtained (Fig. 5). Two inflexions corresponding to deprotonation of both the hydroxyl groups of iron(III)-bound H_2DBC (pK_a: Pip, 2.0; Et_3N, 1.9; uncoordinated H_2DBC, 2.7, 10.2[55]) and $HDBC^-$ (pK_a: Pip, 5.3; Et_3N, 5.1) in two steps are discerned (Scheme 7). This suggests that the coordinated ethanolate is protonated on adding $HClO_4$ and is deprotonated again at high concentrations of base. In the absence of added acid an inflexion corresponding to the deprotonation of bound $HDBC^-$ is observed (pK_a: Pip, 5.5; Et_3N, 5.1) and only half of the inflexion for deprotonation of the first hydroxyl group of

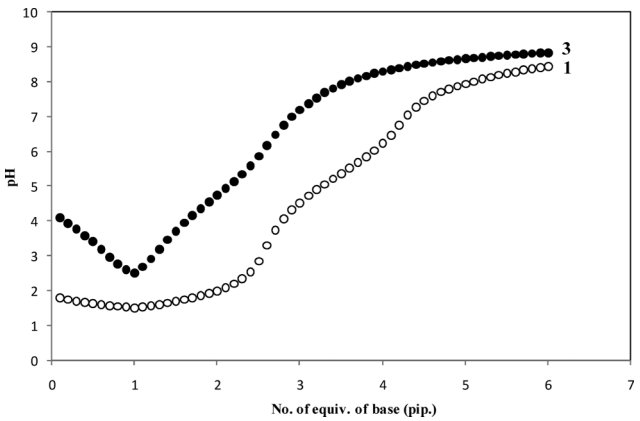

Fig. 5 pH titration of an equimolar mixture of complex **1** and **3** (4×10^{-4} M), $HClO_4$ and H_2DBC against piperidine in methanol solution.

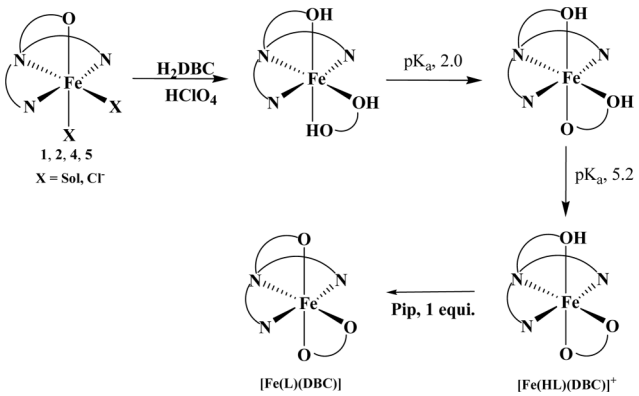

Scheme 7 Catecholate adduct species formed during pH-titration of equimolar quantities of $[Fe(L)Cl_2]$ and H_2DBC.

catechol is discerned (Figure S2, ESI‡), implying that the iron(III)-bound ethanolate has abstracted the proton from H_2DBC bound to iron(III). All these observations reveal that the coordinated ethanolate facilitates deprotonation of H_2DBC upon coordination to iron(III) and so lower amounts of base are needed to generate the adduct species. In acetonitrile solution two distinct inflexions are observed corresponding to deprotonation of the two catechol hydroxyl groups by piperidine in two distinct steps (pK_a, 2.35, 4.95), suggesting that the solvent methanol is not deprotonated. It is interesting that the ability of the iron(III)-bound ethanolate moiety to act as an internal base is analogous to that of the axially bound Tyr447 in 3,4-PCD enzyme. Krebs *et al.* have shown that the iron(III) bound by *N*-acetyl-*N*′,*N*′-bis(2-pyridyl-2-ylmethyl)ethylenediamine (acetyl-uns-penp) acts as an internal base.[47] Yamahara *et al.* used acetylacetonate as an exogeneous ligand in iron(III) complexes to serve as 1.0 equivalent of base upon catecholate coordination.[48] In contrast to **1**, a sharp decrease and then an increase in pH is observed for **3** with added $HClO_4$ during the initial stages of titration (Fig. 5), corresponding to consumption of free acid, and two closely located inflexions (pK_a, 4.7, 5.2,

Table 4 Electrochemical data[a] for Fe^{III}/Fe^{II} redox process of iron(III) complexes and their catecholate adduct in methanol at 25.0 ± 0.2 °C using a scan rate of 50 mV s^{-1} (CV) and 5 mV s^{-1} (DPV)

Complex	E_{pc} (V)	E_{pa} (V)	$E_{1/2}$ (V) CV	$E_{1/2}$ (V) DPV	D × 10^{-6} cm^2 s^{-1}	Redox process
$[Fe(L1)Cl_2]$	0.068	0.164	0.116	0.117	4.5	$Fe^{III} \rightarrow Fe^{II}$
+ H_2DBC	—	—	—	—		DBSQ → H_2DBC
	0.056	0.172	0.114	0.121		$Fe^{III} \rightarrow Fe^{II}$
+ [b]DBC^{2-}	0.056	0.170	0.113	0.120		DBSQ → DBC^{2-}
	—	—	—	—		$Fe^{III} \rightarrow Fe^{II}$
+[c]DBC^{2-}	0.058	0.156	0.107	0.112		DBSQ → DBC^{2-}
	—	—	—	—		$Fe^{III} \rightarrow Fe^{II}$
$[Fe(L2)Cl_2]$	0.104	0.182	0.143	0.125	3.8	$Fe^{III} \rightarrow Fe^{II}$
+ H_2DBC	—	—	—	—		DBSQ → H_2DBC
	0.100	0.200	0.150	0.138		$Fe^{III} \rightarrow Fe^{II}$
+[b]DBC^{2-}	0.098	0.196	0.147	0.130		DBSQ → DBC^{2-}
	—	—	—	—		$Fe^{III} \rightarrow Fe^{II}$
+[c]DBC^{2-}	0.098	0.180	0.139	0.127		DBSQ → DBC^{2-}
	—	—	—	—		$Fe^{III} \rightarrow Fe^{II}$
$[Fe(H(L3))Cl_3]$	0.142	0.200	0.171	0.153	6.6	$Fe^{III} \rightarrow Fe^{II}$
+ H_2DBC	—	—	—	—		DBSQ → H_2DBC
	0.124	0.210	0.167	0.163		$Fe^{III} \rightarrow Fe^{II}$
+[b]DBC^{2-}	0.120	0.202	0.161	0.143		DBSQ → DBC^{2-}
	—	—	—	—		$Fe^{III} \rightarrow Fe^{II}$
+[c]DBC^{2-}	0.140	0.242	0.191	0.145		DBSQ → DBC^{2-}
	—	—	—	—		$Fe^{III} \rightarrow Fe^{II}$
$[Fe(L4)Cl_2]$	0.048	0.128	0.088	0.093	2.5	$Fe^{III} \rightarrow Fe^{II}$
+ H_2DBC	—	—	—	—		DBSQ → H_2DBC
	0.044	0.134	0.089	0.085		$Fe^{III} \rightarrow Fe^{II}$
+[b]DBC^{2-}	0.038	0.134	0.086	0.081		DBSQ → DBC^{2-}
	—	—	—	—		$Fe^{III} \rightarrow Fe^{II}$
+[c]DBC^{2-}	0.022	0.120	0.071	0.079		DBSQ → DBC^{2-}
	—	—	—	—		$Fe^{III} \rightarrow Fe^{II}$
$[(Fe(L5)Cl)_2](ClO_4)_2$[d]	0.032	0.084	0.058	0.038	0.7	$Fe^{III} \rightarrow Fe^{II}$
+ H_2DBC	—	—	—	—		DBSQ → H_2DBC
	—	0.098	—	0.039		$Fe^{III} \rightarrow Fe^{II}$
+[b]DBC^{2-}	0.028	0.096	0.062	0.037		DBSQ → DBC^{2-}
	—	—	—	—		$Fe^{III} \rightarrow Fe^{II}$
+[c]DBC^{2-}	0.026	0.078	0.052	0.031		DBSQ → DBC^{2-}
	—	—	—	—		$Fe^{III} \rightarrow Fe^{II}$

[a] Potential measured *vs.* $Ag/AgNO_3$ (0.01 M, 0.1 M TBAP); add 0.544 V to convert to NHE. [b] Generated by adding proper equivalents (0.7–1.0 equiv.) piperidine to H_2DBC. [c] The amount of complex used was 0.5×10^{-3} M. [d] Generated by adding two equivalents of piperidine.

Scheme 6B) are observed in methanol solution. This reveals that DBC^{2-} is chelated to iron(III) in the equatorial plane[32] with respect to the axially coordinated amine nitrogen. In the absence of added acid, the neutralization point is observed upon adding around half-an-equivalent of base, confirming the tendency of iron(III)-bound H_2DBC towards spontaneous deprotonation. Interestingly, in contrast to methanol solution, two distinct inflexions (pK_a: Pip, 4.7, 5.6) are observed in acetonitrile solution, revealing that DBC^{2-} is coordinated both in the axial and equatorial positions leading to two distinct pK_a values, which has an interesting impact on the catechol cleavage pattern (*cf.* below).

Electrochemical behavior

The electrochemical data obtained for the iron(III) complexes **1–5** and their DBC^{2-} adducts generated *in situ* in methanol solution using TBAP as supporting electrolyte are collected in Table 4. All the complexes exhibit both cathodic (+0.032–0.142 V) and anodic waves (+0.084 –0.200 V) at positive potentials, which are assigned to Fe^{III}/Fe^{II} couple (Fig. 6).[17–22,24,29] The cathodic current functions (D, 0.7–4.5 × 10^{-6} cm^2 s^{-1}) calculated by using Randles-Sevciks' equation[56] are of the same order as those observed for other iron(III) complexes undergoing a diffusion controlled one-electron reduction process.[17–22,29] The $E_{1/2}$ values of Fe^{III}/Fe^{II} redox potentials of the present complexes follow the trend **3** > **2** > **1**; **1** > **4** > **5**, which reflects the decrease in Lewis acidity of the

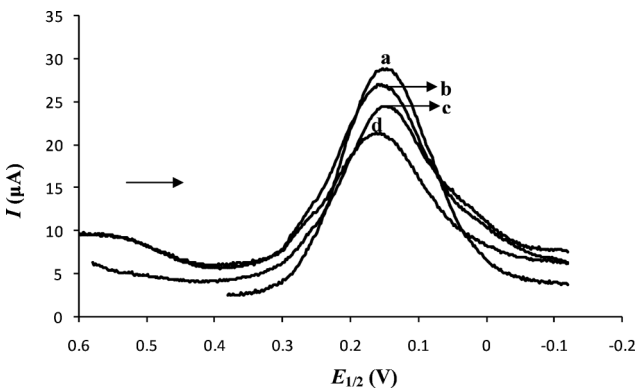

Fig. 6 Differential pulse voltammograms of 1 mM $[Fe(L2)Cl_2]$ **2** (a), with 1 mM H_2DBC added, after addition 0.8 equivalents of piperidine (c) and 2.0 equivalents of pyridine (d) in methanol solution at 25 °C. Supporting electrolyte: 0.1 M TBAP. Scan rate: 0.05 V s^{-1} (CV), 0.005 V s^{-1} (DPV).

iron(III) center along this series (*cf.* above). Upon incorporation of a methylene (–CH_2–) group on the ethanolate moiety in **1** to obtain **2**, the lone pair orbital of the propanolate oxygen atom is not oriented exactly towards the iron(III) orbital because of the increase in chelate ring size from five to six, leading to an increase in positive charge on iron(III) and hence the higher Fe^{III}/Fe^{II} redox potential of **2**.[17–22,24,29] Interestingly, on replacing the ethanolate donor in **1** by the uncoordinated (*cf.* above), long and sterically hindering ethoxyethanol moiety as in **3**, the Fe(III)/Fe(II) redox potential increases due to the increase in positive charge on iron(III). Also, on replacing one/two pyridylmethyl arm(s) in **1** ($E_{1/2}$, + 0.117 V) by one/two 1-methylimidazolylmethyl arms to obtain **4**/**5**, a decrease in redox potential ($E_{1/2}$: **4**, +0.093; **5**, +0.063 V) is observed, which is expected of the higher Lewis basicity[54] of the 1-methylimidazole nitrogen donor.[20,22,29]

Upon adding one equivalent of H_2DBC to **1–5** in methanol solution, the DBSQ/H_2DBC redox wave is overlaid on the Fe(III)/Fe(II) redox wave (+0.038–0.163 V, Fig. 6, DPV) and interestingly, it is not shifted when piperidine is added as base (0.7–1.0 equivalent, +0.037–0.143 V; 2.0 equivalents, +0.031–0.145 V), but a small decrease in reduction current is observed. This suggests that both the catecholate adducts $[Fe(HL)(DBC)]^+$ and [Fe(L)(DBC)] involve the same DBSQ/DBC^{2-} redox process at the same potential, irrespective of whether the catechol is protonated or not. The Fe^{III}/Fe^{II} redox wave is expected to be shifted to a more negative potential due to bidentate coordination of DBC^{2-} (*cf.* above). The DBSQ/DBC^{2-} redox couple is observed at potentials more positive than that of the free couple (E_{pc}, –1.34 V *vs.* SCE), reflecting the significant stabilization of coordinated DBC^{2-} towards oxidation.[56]

Catechol dioxygenase activity

The catecholate adducts were generated *in situ* by treating the complexes **1–5** with equimolar quantities of 3,5-di-*tert*-butylcatechol (H_2DBC) and appropriate equivalents (0.7–2.0) of piperidine as base in methanol solvent. The decay of the low-energy catecholate-to-iron(III) LMCT band (Fig. 7) on oxygenation exhibits pseudo-first order kinetics as judged from the linearity of the plot [1+log(Absorbance)] *vs.* time (Fig. 8) and the values of k_{obs} were calculated from the slopes of these plots. The second order rate constants were calculated[17–22,25,29,33,34,37,53] (Table 5) by using eqn. 1:

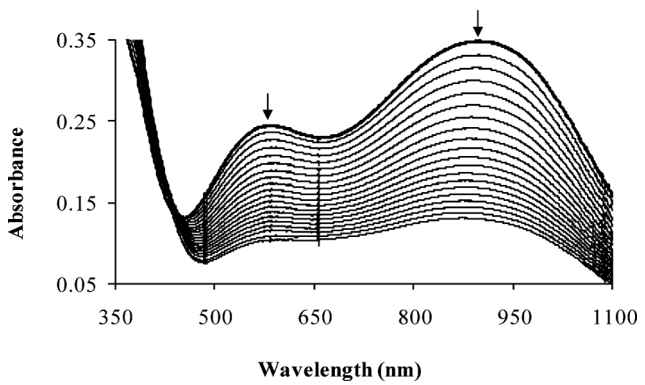

Fig. 7 Progress of the reaction of the adduct $[Fe(H(L3))(DBC)]^+$ with O_2 in methanol solution using 1.0 equivalent of piperidine. The disappearance of the DBC^{2-}-to-iron(III) LMCT band is monitored.

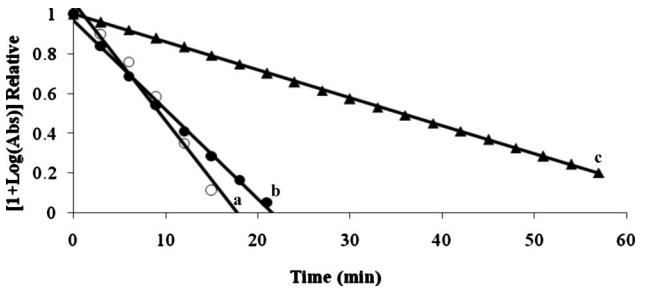

Fig. 8 Plots of [1+log(Absorbance)] *vs.* time for the reaction of $[Fe(HL)(DBC)]^+$, generated by treating the iron(III) complexes with H_2DBC pretreated with 0.7–1.0 equivalent of piperidine, with O_2 at 25 °C in methanol solution. Concentration of the adduct: 2×10^{-4} M. (**a**): $[Fe(HL1)(DBC)]^+$ **1**, (**b**): $[Fe(HL2)(DBC)]^+$ **2**, (**c**): [Fe(H(L3))(DBC)Cl] **3**.

$$k_{O_2} = k_{obs}/[O_2] \quad (1)$$

The DBC^{2-} adducts [Fe(L)(DBC)] of **1**, **2**, and **3** generated *in situ* by using two equivalents of piperidine, reacted with dioxygen over 12 h (> $t_{1/2}$, Table 5) and yielded large amounts of intradiol-cleavage products (**1**, 73.9; **2**, 61.1; **3**, 78.0%), small amounts of quinone (**1**, 12.7; **2**, 13.8; **3**, 5.0%), and extradiol products (**3**, 12.3%) and lesser amount (**1**, 2.2; **2**, 2.3%) of 3-*tert*-butylfuran-2,5-dione (**12**) (Scheme 8).

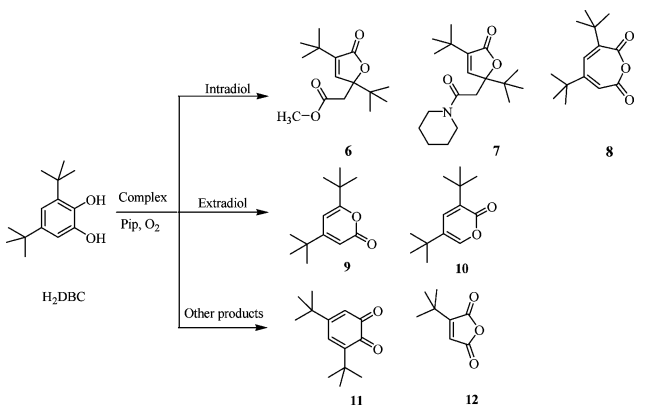

Scheme 8 Products of catechol cleavage of H_2DBC mediated by complexes using **1–5** molecular oxygen: 2,4-di-*tert*-butyl-5-oxo-2,5-dihydrofuran-2-yl)acetic acid methyl ester (**6**), 3,5-di-*tert*-butyl-5-(2-oxo-2-piperidinylethyl)-5*H*-furanone (**7**), 3,5-di-*tert*-butyl-1-oxacycloheptа-3,5-diene-2,7-dione (**8**), 4,6-di-*tert*-butyl-2-pyrone (**9**), 3,5-di-*tert*-butyl-2-pyrone (**10**), 3,5-di-*tert*-butyl-1,2-benzoquinone (**11**), 3-*tert*-butyl-furan-2,5-dione (**12**).

In contrast, the adducts [Fe(L)(DBC)] derived from **4** and **5** (λ_{max}: **4**, 431, 687; **5**, 434, 685 nm) on reaction with O_2 afforded major amounts of the oxidized product benzoquinone (**4**, 45.0; **5**, 75.0%) and small amounts of intradiol-cleavage products (**4**, 32.4; **5**, 8.2%). The formation of intradiol-cleavage products for the catecholate adducts of **1** and **2** is expected of their six-coordinate geometry, which favors the substrate activation[24–29,33–38] (Scheme 9, A3) rather than dioxygen-activation[57,58] pathway, as the latter requires a vacant coordination site on the catecholate adduct for molecular oxygen binding followed by its activation. Also, dioxygen would first attack a carbon site on the octahedral iron(III)-bound catecholate substrate and then bind to the iron(III)

Table 5 Cleavage products obtained (Scheme 6) upon oxygenation and rate of oxygenation reactions of iron(III)-catecholate adduct[a] generated *in situ* in methanol solution

Complexes	Solvent	Piperidine equivalents	Intradiol (%)	Extradiol (%)	Quinone (%)	Other product (%)	Reaction rate ($\times 10^{-1}$ M^{-1} s^{-1})	$t_{1/2}$ (h)[b]
$[Fe(L1)Cl_2]$	MeOH	0.8	14.9 (**6**) 46.4 (**7**) 6.2 (**8**)	—	20.0 (**11**)	10.1 (**12**)	7.70 ± 0.02	0.11
		2.0	73.9 (**7**)	—	12.7 (**11**)	2.2 (**12**)	1.62 ± 0.02	0.53
$[Fe(L2)Cl_2]$	MeOH	0.8	8.4 (**6**) 60.9 (**7**) 3.5 (**8**)	—	9.1 (**11**)	14.4 (**12**)	4.30 ± 0.01	0.20
		2.0	61.1 (**7**)		13.8 (**11**)	2.3 (**12**)	0.94 ± 0.03	0.92
$[Fe(H(L3))Cl_3]$	MeOH	1.0	17.0 (**6**) 56.0 (**7**) 5.1 (**8**)	1.2 (**9**) 4.9 (**10**)	2.7 (**11**)	—	1.40 ± 0.02	0.62
		2.0	78.0 (**7**)	7.5 (**9**) 4.8 (**10**)	5.0 (**11**)	—	0.58 ± 0.01	1.50
	ACN	2.0	24.3 (**7**)	1.0 (**10**)	<1.0 (**11**)	—	—	—
$[Fe(L4)Cl_2]$	MeOH	0.7	17.2 (**6**) 19.6 (**7**) 10.0 (**8**)	—	22.9 (**11**)	3.8 (**12**)	2.30 ± 0.03	0.37
		2.0	1.8 (**6**) 30.6 (**7**)	—	45.0 (**11**)		0.63 ± 0.03	1.38
$[\{Fe(L5)Cl\}_2]^{2+}$	MeOH	0.7	19.1 (**6**) 14.6 (**7**) 8.8 (**8**)	—	45.0 (**11**)	—	0.13 ± 0.04	6.70
		2.0	4.4 (**6**) 3.8 (**7**)	—	75.0 (**11**)	— 5.4 (**12**)	0.16 ± 0.04	5.44

[a] $kO_2 = k_{obs}/[O_2]$. The solubility of O_2 in methanol is taken as 2.21 mM at 25 °C. The kinetic data were obtained by monitoring the disappearance of the low-energy DBC^{2-}-to-iron(III) LMCT band. [b] $t_{1/2} = 0.693/k_{obs}$

center after or before displacing the coordinated semiquinone oxygen donor arm to form a six- or seven-coordinate peroxo intermediate.[59] Also, the formation of both intra- and extradiol-cleavage products for **3** can be explained by acyl and alkenyl migration, respectively, in the reactive substrate-alkylperoxo-Fe^{3+} $[(L)(DBSQ)Fe(III)\text{-}O_2]^-$ intermediate formed in the catalytic cycle (Scheme 9, B2).[28,57,58] The observed result is in agreement with our previous report[21] that iron(III) complexes of facially coordinating tridentate N_3 ligands yield intradiol cleavage products exclusively (80 – 90%), with trace amounts of extradiol product (< 1%) in DMF solvent using piperidine as base.

The adducts of **4** and **5**, like those of **1** and **2**, are expected to give major amounts of intradiol-cleavage products upon oxygenation; however, benzoquinone is mainly obtained by the axial attack of dioxygen on the DBC^{2-} adducts of **4** and **5**, in both of which the displacement of protonated ethanolate arm (coordinated *trans* to catecholate oxygen) from the coordination sphere is facilitated by the coordination of the DBC^{2-} dianion (Scheme 9, A4). The axially bound dioxygen is unable to attack the semiquinone radical located in the same plane to provide extradiol cleavage and hence benzoquinone is formed in larger amounts than for $[Fe(terpy)Cl_3]$, where terpy = 2,2′:6,2′-terpyridine.[60] Also, the more basic (*cf.* above) 1-methylimidazolyl donor(s) strongly bound to iron(III) in the adducts of **4** and **5** facilitates the de-coordination of the ethanolate arm more than the pyridyl donors in the adducts of **1** and **2**, leading to higher quantities of benzoquinone product. Upon replacement of one of the pyridylmethyl arms in $[Fe(TPA)(DBC)]^+$ by an ethanolate/propanolate group to obtain the adducts [Fe(L1)(DBC)]/[Fe(L2)(DBC)], the rate of reaction decreases appreciably and the trends in the reaction rates (1.62–0.16 × 10^{-1} $M^{-1}s^{-1}$) observed for the present complexes are **1** > **2** > **3**; **1** > **4** > **5**. The replacement of one/two of the pyridylmethyl arms in **1** by one/two 1-methylimidazolylmethyl arm as in **4** (0.63 × 10^{-1} M^{-1} s^{-1})/**5** (0.16 ×10^{-1} $M^{-1}S^{-1}$) leads to a decrease in reaction rate, which corresponds mainly to quinone formation.

The decrease[20,22,29] in Lewis acidity of the iron(III) center, effected by incorporating the more basic 1-methylimidazolyl moieties (*cf.* above), results in weaker catecholate binding and also decreased O_2 attack. It is well-known that a higher Lewis acidity of the iron(III) center leads to a higher iron(III)-catecholate covalency and hence a higher reaction rate.[22,27–29] The replacement of the ethanolate arm in **1** by the ethoxyethanol arm, as in **3**, is expected to increase the Lewis acidity of the iron(III) center and hence the reaction rate. However, the reaction rate decreases (0.58 × 10^{-1} M^{-1} s^{-1}), possibly due to chloride coordination (*cf.* above). Among the present catecholate adducts of **1**, **4** and **5**, it is seen that the rate of dioxygenation of the adduct of **5** with the highest energy for the low-energy LMCT band is the lowest and that of adduct of **1** with the lowest LMCT band energy is the highest. This LMCT energy-dependent reactivity can be illustrated[28a] by invoking the spin-inversion phenomenon proposed by Funabiki *et al.*[59] An adduct with a lower energy catecholate-to-iron(III) LMCT band and hence a lower energy for spin-inversion from S = 5/2 to S = 3/2 at the iron(III) centre exhibits a higher rate of oxygenation. The present observation can be elegantly illustrated also by invoking the mechanism proposed very recently by Solomon *et al.*[61] to overcome the spin-forbidden nature of the reaction between the triplet O_2 and spin-singlet of the organic substrate. Thus, the transfer of α spin in the d_{xz} orbital of iron(III) to the O_2 molecule is facilitated in **1** as this orbital is destabilized because of accumulation of electron density on iron(III) more by the ethanolate rather than the propanolate oxygen donor. Also,

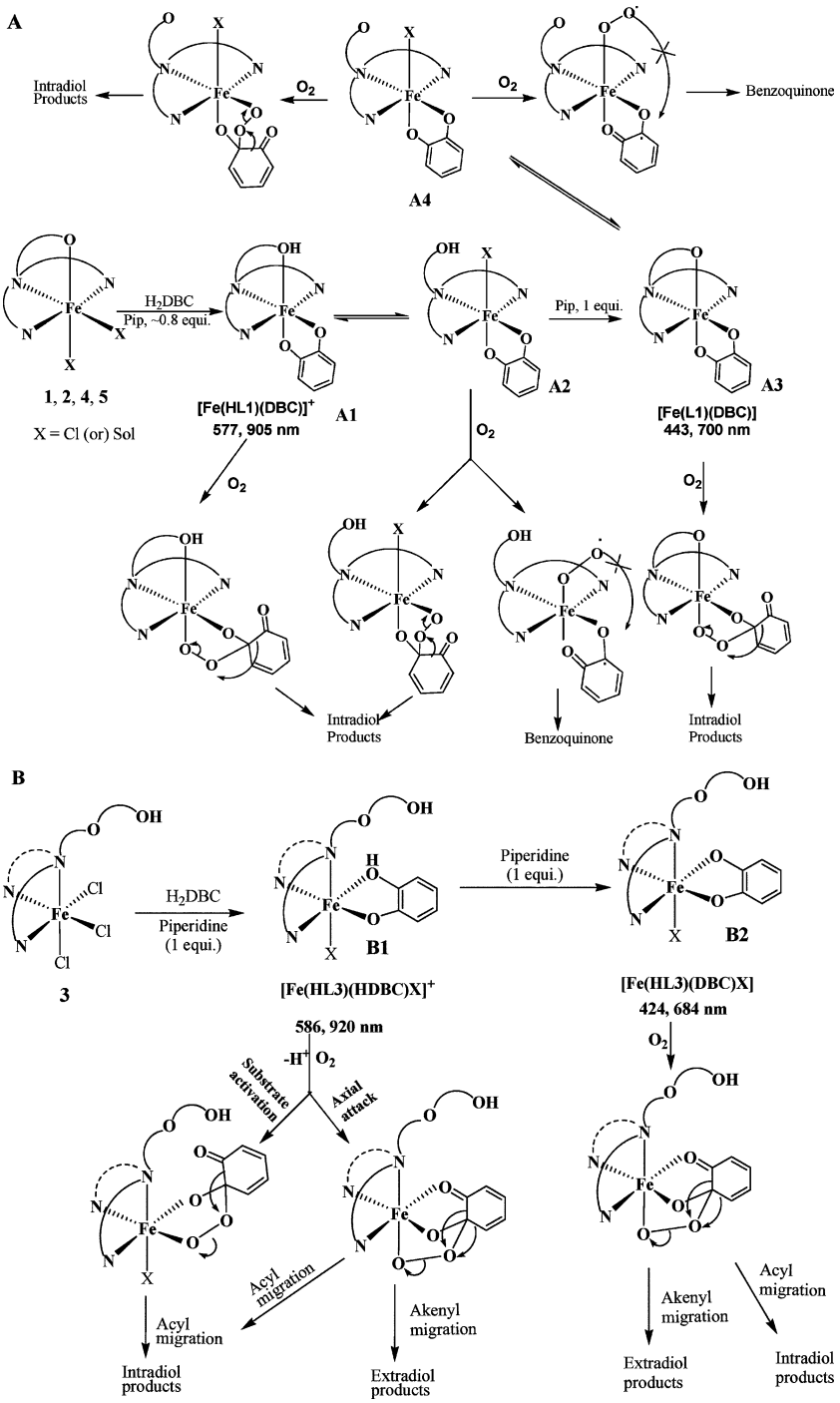

Scheme 9 Proposed pathways for the formation of intra- and extradiol-cleavage and benzoquinone products.

when the ligand donor arm is varied from pyridylmethyl (**1**) to imidazolylmethyl (**4**, **5**), the electron density on the iron(III) center decreases, leading to a decrease in the reaction rate.

It would be interesting to study the reactivity of the $[Fe(HL)(DBC)]^+$ and $[Fe(HL3)(HDBC)X]^+$ adducts, discerned in the electronic absorption spectral study. These adducts were generated *in situ* by using 0.7–1.0 equivalent of piperidine in methanol and reacted with dioxygen over a period of 6 h ($> t_{1/2}$, Table 5) to afford intradiol-cleavage products (I) in the following amounts: **1**, 67.5; **2**, 72.8; **3**, 78.1; **4**, 46.8; **5**, 42.5%; smaller amounts of the oxidized product benzoquinone (Q) in the following amounts: **1**, 20.0; **2**, 9.1; **3**, 2.7; **4**, 22.9; **5**, 45.0%; and small amounts (3.8–14.4%) of 3-*tert*-butylfuran-2,5-dione as a side product. Interestingly, only a very small amount of extradiol products (6.1%) is observed for **3**. The observation of mainly intradiol-cleavage products for the catecholate adducts $[Fe(HL)(DBC)]^+$ is illustrated by invoking substrate-activation[24–29,33–38] pathway (Scheme 9, A1). The formation of intra- and extradiol-cleavage products for **3** is explained by acyl and alkenyl migration in the reactive substrate-alkylperoxo-Fe^{3+} intermediate $[(L)(DBSQ)Fe(III)O_2]^-$ formed by the axial

attack of O_2 (Scheme 9, B1).[28,57,58] Also, it is interesting that the adducts $[Fe(HL4)(DBC)]^+$ (I/Q, 2.0) and $[Fe(HL5)(DBC)]^+$ (I/Q, 1.0) yield intradiol-cleavage products in higher amounts than the [Fe(L)(DBC)] adducts of **4** (I/Q, 0.7) and **5** (I/Q, 0.1).

The concerted attack of dioxygen on the iron(III)-catecholate adducts of **4** and **5**, both with the protonated ethanolate arm of the ligand displaced from the coordination sphere (Scheme 9, A2), is facilitated to provide higher amounts of intradiol-cleavage products. Also, the axially bound dioxygen is unable to attack the semiquinone radical located in the same plane and hence the oxidation product benzoquinone is also formed, but in smaller quantities.[60] Thus, it is interesting that the $[Fe(HL)(DBC)]^+$ adducts with a solvated site facilitates the concerted attack of O_2 and hence the intradiol-cleavage of catechol and that the changes in the coordination sphere caused upon substrate binding are similar to those in catechol dioxygenase enzymes.

Remarkably, the rate of oxygenation ($7.7–0.13 \times 10^{-1}$ M^{-1} s^{-1}) observed for the $[Fe(HL)(DBC)]^+$ adducts, except $[Fe(HL5)(DBC)]^+$, are 3–5 fold higher than that for [Fe(L)(DBC)] adducts. The iron(III)-catecholate interaction in these adducts is more asymmetric[24,25,27–29] than in [Fe(L)(DBC)]/[Fe(HL3)(DBC)X] adducts, as indicated by the higher values of $\Delta\lambda_{max}$ observed for them (*cf.* above), conferring higher reaction rates with higher amounts of intradiol products. Also, the Lewis acidity of the iron(III) center (*cf.* above) in $[Fe(HL)(DBC)]^+$ adducts is higher than that in the respective [Fe(L)(DBC)] adducts and a vacant coordination position (*cf.* above) is available for concerted attack of dioxygen. Also, the observed trends in rate of oxygenation of $[Fe(HL)(DBC)]^+$ (**1** > **2** > **3**; **1** > **4** > **5**) are the same as those for [Fe(L)(DBC)]. The catecholate adduct of **3** exhibits the low energy DBC^{2-}-to-iron(III) LMCT band at the lowest energy among the present adducts, but it displays a lower reaction rate, possibly because both the intra- and extradiol cleavage pathways contribute to the overall rate observed.[30]

Thus the catecholate adducts $[Fe(HL)(DBC)]^+$ act as excellent biomimetic models for intradiol-cleaving catechol dioxygenases and the ethanolate/propanolate donor mimics the function of axially bound Tyr447 in 3,4-PCD enzyme. The higher Lewis acidity of the iron(III) center in these catecholate adducts, as determined by the electronic effects of ligand donors, enhances the catecholate-iron(III) interaction and dictates the mode and yield of catechol cleavage products as well as the rate of dioxygenation. Interestingly, the nature of the solvent has the ability to change the mode of binding of catechol substrate and hence the product selectivity.

Conclusions

In the X-ray structures of two of the iron(III) complexes of the tripodal tetradentate N_3O ligand the ethanolate oxygen is coordinated to iron(III), while in the complex of the facially coordinating N_3O_2 ligand the ethoxyethanol moiety is not coordinated. The adduct species [Fe(L)(DBC)] generated in methanol solution with two equivalents of piperidine contain the deprotonated alkoxide donor, as revealed by the higher energies of both the DBC^{2-}-to-iron(III) LMCT bands. Upon replacing one/two pyridylmethyl arm(s) of the tripodal ligands in these adducts by imidazolylmethyl arm(s), the LMCT band energy decreases, and remarkably, higher amounts of benzoquinone and lower amounts of intradiol cleavage product are observed. The iron(III) complexes interact with H_2DBC in the presence of one equivalent of piperidine to form the adduct $[Fe(HL)(DBC)]^+$, in which the coordinated alkoxide donor of the ligand has abstracted a proton of the catechol. Remarkably, these adducts afford larger quantities of intradiol-cleavage products and lesser amounts of benzoquinone and react faster than [Fe(L)(DBC)] adducts. Thus, the alkoxide-bound iron(III) complexes have the potential to abstract a proton from the catechol substrate and serve as excellent biomimetic model systems for mimicking the acid–base function of axially-bound Tyr447 of intradiol-cleaving catechol dioxygenase enzymes.

Acknowledgements

We sincerely thank the Council of Scientific and Industrial Research, New Delhi, for Senior Research Fellowships to K.S. and M.S. We thank the Department of Science and Technology (DST), New Delhi, for supporting this research [Scheme No. SR/S1/IC-45/2003 and SR/S5/BC-05/2006]. Professor M. Palaniandavar is a recipient of a Ramanna Fellowship [Scheme No. SR/S1/RFIC-01/2010] from DST, New Delhi. We thank Professor K. Natarajan, Bharathiar University, Coimbatore, for CHN analysis.

References

1 (*a*) E. I. Solomon, A. Decker and N. Lehnert, *Proc. Natl. Acad. Sci. U. S. A.*, 2003, **100**, 3589; (*b*) E. I. Solomon, T. Burnold, M. I. Davis, J. N. Kemsley, S.-K. Lee, N. Lehnert, F. Neese, A. J. Skulan, Y.-S. Yang and J. Zhou, *Chem. Rev.*, 2000, **100**, 235; (*c*) R. H. Holm, P. Kennepohl and E. I. Solomon, *Chem. Rev.*, 1996, **96**, 2239.
2 L. P. Wackett, *Enzyme Microb. Technol.*, 2002, **31**, 577.
3 L. Que, Jr. and R. Y. N. Ho, *Chem. Rev.*, 1996, **96**, 2607.
4 F. H. Vaillancourt, J. T. Bolin and L. D. Eltis, In *Pseudomonas*, J.-L. Ramos ed. Kluwer/Plenum, New York, 2004, p 359–395.
5 C. J. Schofield and Z. Zhang, *Curr. Opin. Struct. Biol.*, 1999, **9**, 722.
6 O. Hayaishi, M. Katagiri and S. Rothberg, *J. Am. Chem. Soc.*, 1955, **77**, 5450.
7 D. H. Ohlendorf, J. D. Lipscomb and P. C. Weber, *Nature*, 1988, **336**, 403.
8 (*a*) D. H. Ohlenddorf, A. M. Orville and J. D. Lipscomb, *J. Mol. Biol.*, 1994, **244**, 586; (*b*) T. E. Elgren, A. M. Orville, K. A. Kelly, J. D. Lipscomb, D. H. Ohlendorf, L. Que and Jr, *Biochemistry*, 1997, **36**, 11504.
9 M. W. Vetting, C. A. Earhart and D. H. Ohlendorf, *J. Mol. Biol.*, 1994, **236**, 372.
10 (*a*) M. Y. M. Pau, M. I. Davis, A. M. Orville, J. D. Lipscomb and E. I. Solomon, *J. Am. Chem. Soc.*, 2007, **129**, 1944; (*b*) L. Shu, Y. M. Chiou, A. M. Orville, M. A. Miller, J. D. Lipscomb and L. Que, Jr., *Biochemistry*, 1995, **34**, 6649.
11 S. Han, L. D. Eltis, K. N. Timmis, S. W. Muchmore and J. T. Bolin, *Science*, 1995, **270**, 976.
12 A. Kita, S. I. Kita, I. Fujisawa, K. Inaka, T. Ishida, K. Horiike, M. Nozaki and K. Miki, *Structure*, 1998, **7**, 25.
13 (*a*) K. Sugimoto, T. Senda, H. Aoshima, E. Masai, M. Fukuda and Y. Mitsui, *Structure*, 1999, **7**, 953; (*b*) K. Sugiyama, T. Senda, H. Narita, T. Yamamoto, K. Kimbara, M. Fukuda, K. Yano and Y. Mitsui, *Proc. Jpn. Acad., Ser. B, Phys. Biol. Sci.*, 1995, **B71**, 32.
14 G. P. Titus, H. A. Mueller, J. Burgner, S. Rodriguez de Cordoba, M. A. Penalva and D. E. Timm, *Nat. Struct. Biol.*, 2000, **7**, 542.
15 (*a*) M. I. Davis, E. C. Wasinger, A. Decker, M. Y. M. Pau, F. H. Vaillancourt, J. T. Bolin, L. D. Eltis, B. Hedman, K. O. Hodgson and E. I. Solomon, *J. Am. Chem. Soc.*, 2003, **125**, 11214; (*b*) F. H. Vaillancourt, J. T. Bolin and L. D. Eltis, *Crit. Rev. Biochem. Mol. Biol.*, 2006, **41**, 241.
16 L. Que Jr., J. D. Lipscomb, E. Munch and J. M. Wood, *Biochim. Biophys. Acta*, 1977, **485**, 60.

17 R. Viswanathan, M. Palaniandavar, T. Balasubramanian and P. T. Muthiah, *J. Chem. Soc., Dalton Trans.*, 1996, 2519.
18 R. Viswanathan, M. Palaniandavar, T. Balasubramanian and P. T. Muthiah, *Inorg. Chem.*, 1998, **37**, 2943.
19 (*a*) M. Velusamy, M. Palaniandavar, R. Srinivasagopalan and G. U. Kulkarni, *Inorg. Chem.*, 2003, **42**, 8283; (*b*) R. Mayilmurugan, M. Sankaralingam, E. Suresh and M. Palaniandavar, *Dalton Trans.*, 2010, **30**, 9611.
20 M. Velusamy, R. Mayilmurugan and M. Palaniandavar, *Inorg. Chem.*, 2004, **43**, 6284.
21 M. Velusamy, R. Mayilmurugan and M. Palaniandavar, *J. Inorg. Biochem.*, 2005, **99**, 1032.
22 (*a*) M. Pascaly, M. Duda, F. Schweppe, K. Zurlinden, F. K. Muller and B. Krebs, *J. Chem. Soc., Dalton Trans.*, 2001, 828; (*b*) M. Pascaly, C. Nazikkol, F. Schweppe, A. Wiedemann, K. Zuilinden and B. Krebs, *Z. Anorg. Allg. Chem.*, 2000, **626**, 50; (*c*) M. Merkel, M. Pascaly and B. Krebs, *Inorg. Chem.*, 2005, **44**, 7582; (*d*) M. Pascaly, M. Duda, A. Rompel, B. H. Sift, W. Meyer-Klaucke and B. Krebs, *Inorg. Chim. Acta*, 1999, **219**, 289.
23 S. Ogo, R. Yamahara, T. Funabiki, H. Masuda and Y. Watanabe, *Chem. Lett.*, 2001, 1062.
24 D. D. Cox, L. Que and Jr, *J. Am. Chem. Soc.*, 1988, **110**, 8085.
25 D. D. Cox, S. J. Benkovic, L. M. Bloom, F. C. Bradley, M. J. Nelson, L. Que and Jr, *J. Am. Chem. Soc.*, 1988, **110**, 2026.
26 H. G. Jang, D. D. Cox and L. Que, Jr., *J. Am. Chem. Soc.*, 1991, **113**, 9200.
27 (*a*) R. Viswanathan and M. Palaniandavar, *J. Chem. Soc., Dalton Trans.*, 1995, 1259; (*b*) T. Dhanalakshmi, M. Bhuvaneshwari and M. Palaniandavar, *J. Inorg. Biochem.*, 2006, **100**, 1527.
28 (*a*) K. Visvaganesan, R. Mayilmurugan, E. Suresh and M. Palaniandavar, *Inorg. Chem.*, 2007, **46**, 10294; (*b*) K. Sundaravel, T. Dhanalakshmi, E. Suresh and M. Palaniandavar, *Dalton Trans.*, 2008, 7012; (*c*) T. Dhanalakshmi, E. Suresh and M. Palaniandavar, *Dalton Trans.*, 2009, 8328.
29 R. Mayilmurugan, K. Visvaganesan, E. Suresh and M. Palaniandavar, *Inorg. Chem.*, 2009, **48**, 8771.
30 R. Mayilmurugan, E. Suresh and M. Palaniandavar, *Inorg. Chem.*, 2007, **46**, 6284.
31 M. Palanaiandavar and R. Mayilmurugan, *C. R. Chim.*, 2007, **10**, 366.
32 R. Mayilmurugan, H. Stoeckli-Evans and M. Palaniandavar, *Inorg. Chem.*, 2008, **47**, 6645.
33 W. O. Koch, V. Schünemann, M. Gerdan, A. X. Trautwein and H. Krüger, *Chem.–Eur. J.*, 1998, **4**, 1255.
34 (*a*) N. Raffard, R. Carina, A. J. Simaan, J. Sainton, E. Riviere, L. Tchertanov, S. Bourcier, G. Bouchoux, M. Delroisse, F. Banse and J. Girerd, *Eur. J. Inorg. Chem.*, 2001, 2249; (*b*) P. Mialane, L. Tehertanov, F. Banse, J. Sainton and J. Girerd, *Inorg. Chem.*, 2000, **39**, 2440.
35 M. Costas, M. P. Mehn, M. P. Jensen, L. Que and Jr, *Chem. Rev.*, 2004, **104**, 939.
36 T. Funabiki, A. Mizoguchi, T. Sugimoto, S. Tada, M. Tsugi, H. Sakamoto and S. Yoshida, *J. Am. Chem. Soc.*, 1986, **108**, 2921.
37 P. C. A. Bruijnincx, M. Lutz, A. L. Spek, W. R. Hagen, G. Koten and R. J. M. Gebbink, *Inorg. Chem.*, 2007, **46**, 8391.
38 F. Li, M. Wang, P. Li, T. Zhang and L. Sun, *Inorg. Chem.*, 2007, **46**, 9364.
39 D. T. Sawyer, A. Sobkowiak and J. L. Roberts, Jr., *Electrochemistry for Chemists*: 2nd ed. A wiley - Interscience Publication, New York, 1995, p 336.
40 (*a*) S. I. Kirin, C. M. Happel, S. Hrubanova, T. Weyhermüller, C. Klein and N. Metzler-Nolte, *Dalton Trans.*, 2004, 1201; (*b*) J. T. Groves and I. O. Kady, *Inorg. Chem.*, 1993, **32**, 3868.
41 A. F. Abdel-Magid, K. G. Carson, B. D. Harris, C. A. Maryanoff and R. D. Shah, *J. Org. Chem.*, 1996, **61**, 3849.
42 M. Velusamy, M. Palaniandavar, Unpublished results.
43 *SMART & SAINT Software Reference manuals, version 5.0*, Bruker AXS Inc., Madison, WI, 1998.
44 G. M. Sheldrick, *SADABS software for empirical absorption correction*, University of Göttingen, Germany, 2000.
45 *SHELXTL Reference Manual, version 5.1*, Bruker AXS Inc., Madison, WI, 1998.
46 M. Merkel, D. Schnieders, S. M. Baldeau and B. Krebs, *Eur. J. Inorg. Chem.*, 2004, 738.
47 J-Y. Xu, J. Astner, O. Walter, F. W. Heinemann, S. Schindler, M. Merkel and B. Krebs, *Eur. J. Inorg. Chem.*, 2006, 1601.
48 R. Yamahara, S. Ogo, Y. Watanabe and T. Funabiki, *Inorg. Chim. Acta*, 2000, **300-302**, 587.
49 (*a*) D. T. Sawyer, *Oxygen Chemistry*, Oxford University Press, New York, 1991; (*b*) R. Battino, *Oxygen and Ozone*, ed., R. Battino, Pergamon Press, New York, 1981, vol. 7; (*c*) *Kagaku-Binran Basic, Part II*, Second ed., Japan Chemical Society, Tokyo, Japan, 1975.
50 (*a*) M. C. Rodriguez, F. Lambert, I. Morgenstern-Badarau, M. Cesario, J. Guilhem, B. Keita and L. Nadjo, *Inorg. Chem.*, 1997, **36**, 3525; (*b*) D. Mandon, A. Nopper, T. Litrol and S. Goetz, *Inorg. Chem.*, 2001, **40**, 4803; (*c*) K. B. Jensen, C. J. McKenzie, O. Simonsen, H. Toftlund and A. Hazell, *Inorg. Chim. Acta*, 1997, **257**, 163; (*d*) H. Adams, N. A. Bailey, J. D. Crane, D. E. Fenton, J-M. Latour and J-M. Williams, *J. Chem. Soc., Dalton Trans.*, 1990, 1727.
51 E.-Q. Gao, L-H. Yin, J-K. Tang, P. Cheng, D-Z. Liao, Z-H. Jiang and S-P. Yan, *Polyhedron*, 2001, **20**, 669.
52 S. Menage and L. Que, Jr., *Inorg. Chem.*, 1990, **29**, 4293.
53 A. Dei, D. Gatteschi and L. Pardi, *Inorg. Chem.*, 1993, **32**, 1389.
54 R. M. Acheson, *An Introduction to the Chemistry of Heterocyclic Compounds*, Wiely, New York, 1976, p.335.
55 R. B. Jordan and Jin-Huang Xu, *Pure Appl. Chem.*, 1988, **60**, 1205.
56 E. J. Nanni, M. D. Stallings and D. T. Sawyer, *J. Am. Chem. Soc.*, 1980, **102**, 4481.
57 (*a*) E. G. Kovaleva and J. D. Lipscomb, *Science*, 2007, **316**, 453; (*b*) E. G. Kovaleva, M. B. Neibergall, S. Chakrabarty and J. D. Lipscomb, *Acc. Chem. Res.*, 2007, **40**, 475; (*c*) E. G. Kovaleva and J. D. Lipscomb, *Biochemistry*, 2008, **47**, 11168.
58 (*a*) T. D. H. Bugg, *Tetrahedron*, 2003, **59**, 7075; (*b*) G. Lin, G. Reid and T. D. H. Bugg, *J. Am. Chem. Soc.*, 2001, **123**, 5030.
59 Y. Hitomi, M. Yoshida, Y. Higuchi, H. Minami, T. Tanaka and F. Funabiki, *J. Inorg. Biochem.*, 2005, **99**, 755.
60 D. H. Jo and L. Que, Jr., *Angew. Chem., Int. Ed.*, 2000, **39**, 4284.
61 M. Y. M. Pau, J. D. Lipscomb and E. I. Solomon, *Proc. Natl. Acad. Sci. U. S. A.*, 2007, **104**, 18355.

